frontiers in Materials

TYPE Original Research
PUBLISHED 14 April 2026
DOI 10.3389/fmats.2026.1764261

OPEN ACCESS

EDITED BY
Caroline Solazzo,
Independent, United States

REVIEWED BY
Gilliane Monnier,
University of Minnesota Twin Cities, United States
Vadim Parfenov,
Saint Petersburg Electrotechnical University "LETI", Russia

*CORRESPONDENCE
Lauren Lien,
lauren.lien@uliege.be

RECEIVED 10 December 2025
REVISED 27 February 2026
ACCEPTED 04 March 2026
PUBLISHED 14 April 2026

CITATION
Lien L, Cnuts D and Rots V (2026) Tracking the chemical life histories of spruce resin-beeswax mixtures through degradation experiments using reflectance-mode FTIR.
Front. Mater. 13:1764261.
doi: 10.3389/fmats.2026.1764261

Tracking the chemical life histories of spruce resin-beeswax mixtures through degradation experiments using reflectance-mode FTIR

Lauren Lien[1]*, Dries Cnuts[1] and Veerle Rots[1,2]

[1]TraceoLab/Prehistory, University of Liège, Liège, Belgium, [2]F.R.S.-FNRS, Brussels, Belgium

Within residue analysis, experimental degradation studies provide a critical bridge between pristine, modern-day reference materials and the altered residues encountered archaeologically. Here we report on outcomes of a 3-year burial experiment involving spruce resin-beeswax adhesives recovered from cave, loess, sandy, forested, and surface contexts. Reflectance-mode Fourier transform infrared spectroscopy (FTIR) was used to document chemical trajectories across nine specimens using pristine reference materials as baselines. Results show that signals from beeswax are generally resilient, while those from spruce resin are more unstable and frequently weakened or replaced by carboxylate bands. These observations are compatible with progressive hydrolysis and the formation of metal carboxylates, or soap salts. Carbonate and hydroxyl bands further reflect environment-associated inputs, though patterns are inconsistent within depositional categories, potentially reflecting micro-environmental heterogeneity. A pilot principal component analysis (PCA) provides exploratory visualization of environment-associated patterning under specific pre-processing strategies but is sensitive to data treatment, underscoring the risk of potential overfitting given the scope of available data. Collectively, these findings illustrate how FTIR can detect both preserved and transformed adhesive signatures, while also emphasizing the need for non-deterministic interpretive frameworks that account for taphonomic variability. The approach and caveats outlined here aim to strengthen the methodological foundation for residue analysis in archaeology by demonstrating how experimental degradation datasets can refine spectral interpretation of archaeological adhesives.

KEYWORDS
adhesives, degradation, FTIR, spectroscopy, stone tools

1 Introduction

Adhesives represent a key technological innovation within human prehistory. Such adaptations and manipulations of natural resources enabled the hafting of stone tools and the manufacture of composite implements, massively improving the efficiency, precision, and reliability of technological toolkits, ultimately transforming subsistence and craft (e.g., Hardy et al., 2001; Regert, 2004; Rots, 2003; Williamson, 2004; Mazza et al., 2006; Lombard, 2007; 2008; Wadley, 2010; Rots, 2010; Wragg Sykes, 2015; Rots et al., 2016; Degano et al., 2019; Langejans et al., 2022). The selection and manipulation of materials involved in adhesive manufacture require sophisticated

knowledge of material properties, experimentation, and planning depth, often interpreted to reflect both cultural and cognitive advances that extend beyond simple or opportunistic use of natural resources (Charrié-Duhaut et al., 2013; Kozowyk et al., 2017; Hardy et al., 2020; Kozowyk et al., 2020; Langejans et al., 2022; Schmidt and Koch, 2024; Kozowyk et al., 2025). Other research suggests that some adhesive production techniques, such as birch tar synthesis, may be less complex than previously thought, and can be achieved through relatively simple processes requiring little investment (Schmidt et al., 2019). This indicates that the technological and behavioral implications of adhesive production likely varied depending on the materials, methods, and contexts involved.

Organic residues, including adhesives, are highly susceptible to post-depositional alteration and degradation (Eglinton and Logan, 1991; Schwarze, 2007; Wilson et al., 2007; Turner-Walker, 2008; Weiner, 2010; Karkanas, 2010; Lebon et al., 2010; Daher and Bellot-Gurlet, 2013; Pechal et al., 2013; Teacă et al., 2013; Huisman et al., 2017; Pokines et al., 2018; Degano et al., 2019; Filopoulou et al., 2021; Huber et al., 2022; Scaggion et al., 2024). Once discarded, they are immediately subjected to physical, chemical, and biological processes, including oxidation (Eglinton and Logan, 1991; Karkanas et al., 2000; Weiner et al., 2002; Turner-Walker, 2008), hydrolysis (Evershed, 1993; Karkanas et al., 2000; Nielsen-Marsh and Hedges, 2000; Weiner et al., 2002; Wilson and Pollard, 2002), microbial breakdown (Child, 1995; Nicholson 1998; Schwarze, 2007; Pechal et al., 2013; Huisman et al., 2017; Hutschenreuther et al., 2017), and mineralization (Goldberg and Nathan, 1975; Karkanas et al., 2000; Weiner et al., 2002; Lebon et al., 2010; Ortega-Villamagua et al., 2020; Huber et al., 2022; Suosaari et al., 2022; Scaggion et al., 2024; Toffolo, 2025), which can profoundly transform the original composition and physical appearance of a residue. These transformations, as well as contamination, may obscure traditional molecular markers of materials used for identification, significantly complicating their detection and interpretation in archaeological contexts (Haslam, 2004; Haslam, 2006; Columbini and Modugno, 2009; Monnier et al., 2013; Pedergnana et al., 2016; Čížová et al., 2019; Mazurek et al., 2019; Pedergnana, 2020; Frahm et al., 2022; Huber et al., 2022; Zurro and Gadekar, 2024). Residue preservation on stone tools additionally involves taphonomic pathways distinct from those affecting other organic materials. Their intimate contact with the lithic surface results in degradation governed by both environmental chemistry and surface-dependent variables such as texture, porosity, and orientation of the tool within the burial matrix, all of which mediate exposure to oxygen, moisture, and microbial activity (Shanks et al., 2001; Burroni et al., 2002; Cnuts and Rots, 2018; Croft et al., 2018; Hayes and Rots, 2019; Michel et al., 2019). Experimental studies using controlled burial and climate chamber conditions further demonstrate that residue alteration reflects the combined influence of environment and surface-mediated processes (Croft et al., 2016; Michel et al., 2019; Michel and Rots, 2022; Cnuts and Rots, 2024).

Understanding the degradation pathways that affect organic materials is essential to reconstructing ancient adhesive technologies accurately (Evershed, 1993; Wilson and Pollard, 2002; Evershed, 2008; Weiner, 2010; Langejans, 2010; Daher and Bellot-Gurlet, 2013; Briggs and Summons, 2014; Kozowyk et al., 2020; Izzo et al., 2021; Filopoulou et al., 2021; Huber et al., 2022; Gregory and Matthiesen, 2023). Sediment chemistry, pH, hydrology, and microbial communities may strongly influence the pace and nature of post-depositional transformations (Karkanas et al., 2000; Nielsen-Marsh and Hedges, 2000; Weiner et al., 2002; Weiner, 2010; Karkanas, 2010; Huisman et al., 2017; Łucejko et al., 2018; Pokines et al., 2018; Kozowyk et al., 2020; Ortega-Villamagua et al., 2020; Huber et al., 2022; Gregory and Matthiesen, 2023). The period immediately following burial is particularly critical, as degradation processes tend to be most intense during the initial weeks of degradation, when residues encounter fluctuating moisture, oxygenation, and microbial activity (Collins et al. 1995; Denys, 2002; Langejans, 2010; Croft et al., 2016; Michel et al., 2019; Michel and Rots, 2022; Cnuts and Rots, 2024). Subsequent stabilization often reflects changes in sediment chemistry and microenvironmental equilibrium that occurs as the system matures (Gregory and Matthiesen, 2023).

Cave environments often promote carbonate precipitation and mineral encrustation (Goldberg and Nathan, 1975; Karkanas et al., 2000; Karkanas et al., 2002; Weiner et al., 2002; Karkanas, 2010; Lebon et al., 2010). Microbial activity is generally lower in caves than open-air soils because of limited nutrient inputs, cooler temperatures, and reduced oxygenation (Child, 1995; Nicholson 1998; Karkanas, 2010; Weiner, 2010; Huisman et al., 2017). By contrast, sandy and loessic open-air contexts tend to favor oxidative chemistry and microbial infiltration (Burroni et al., 2002; Haslam, 2004; High et al., 2015; Gregory and Matthiesen, 2023). These deposits are well drained and oxygen-rich, creating conditions for oxidation of organic compounds and for microbial communities to colonize residues more actively. Their limited buffering capacity also makes them more susceptible to pH fluctuations and moisture cycling, which can accelerate degradation and leaching of both organics and minerals (Nielsen-Marsh and Hedges, 2000; Haslam, 2004; High et al., 2015; Pokines et al., 2018; Gregory and Matthiesen, 2023).

Fourier transform infrared spectroscopy (FTIR) provides a unique platform for interpreting the chemical makeup of archaeological residues (Shillito et al., 2009; Lebon et al., 2010; Tappert et al., 2011; Bruni and Guglielmi, 2014; Prinsloo et al., 2014; Beltran, 2016; Beltran et al., 2016; Monnier et al., 2017; Langejans et al., 2022; Kozowyk et al., 2025). Unlike gas chromatography-mass spectrometry (GC/MS) or Raman spectroscopy, which generally require destructive sampling or sampling pre-treatment, reflectance-mode FTIR enables non-destructive, *in situ* analysis of organic and mineral deposits directly on stone tool surfaces, allowing us the opportunity to probe the changes caused by degradation at the molecular level while maintaining sample integrity for future analysis (Monnier et al. 2018; Daher et al., 2013; Prinsloo et al., 2014; Monnier et al., 2017; Croft, 2021). By targeting characteristic vibrational markers of beeswax and plant resins, FTIR can detect original constituents and emergent degradation products, such as carboxylates or hydroxyl groups, formed during oxidative and hydrolytic processes (Table 1) (Evershed, 1993; Lebon et al., 2010; Bruni and Guglielmi, 2014; Helwig et al., 2014; Baales et al., 2017; Monnier et al., 2017; Martín Ramos et al., 2018; Mazurek et al., 2019; Tanner and Lichtenberg-Kraag, 2019). This capability is especially relevant for compound adhesives which consist of multiple ingredients that each follow

distinct degradation pathways and exhibit different resistances to environmental stressors. FTIR's potential to resolve overlapping spectral features makes it well suited to investigating how these components interact and transform through time, providing a means to trace the differential degradation of complex mixtures at the molecular level (Shillito et al., 2009; Daher et al., 2013; Prinsloo et al., 2014; Monnier et al., 2017; Monnier & May 2019). However, most existing reference libraries are based on pristine substances, limiting interpretive power in archaeological contexts where materials have been mixed or exposed to various post-depositional processes (Daher and Bellot-Gurlet, 2013; Monnier et al., 2017; Monnier & May 2019; Croft, 2021). A few exceptions, such as the datasets developed by the Helen and Martin Kimmel Center for Archaeological Science Infrared Spectra Library (Weizmann Institute of Science) and the University of Minnesota Archaeological Materials Infrared Spectra Library, include examples of archaeological materials, these remain rare and limited in scope. Unfortunately, many examples of archaeological FTIR data are not made available in accessible digital formats, limiting opportunities for re-analysis, cross-comparison, and collaborative database development. Moreover, systematic spectral libraries for reflectance-mode FTIR are still lacking, even as this becomes a more prominent approach for residue studies. Because spectra obtained in reflectance-mode and transmission mode are fundamentally different and significant processing steps are required for comparability, one-to-one comparisons remain imperfect. Further development of dedicated reflectance-mode reference collections is essential to improve reproducibility and reliability in archaeological residue analysis.

Experimental approaches to residue degradation help bridge this gap (Denys, 2002; Croft et al., 2016; Cnuts and Rots, 2018; Cnuts et al., 2018; Pokines et al., 2018; Michel et al., 2019; Monnier & May 2019; Kozowyk et al., 2020; Michel and Rots, 2022; Cnuts et al., 2022; Cnuts and Rots, 2024). Such studies can be broadly divided into two categories: controlled experiments, conducted in laboratory settings where environmental variables such as temperature, humidity, and UV exposure are regulated to isolate specific mechanisms of degradation (e.g., Michel et al., 2019; Michel and Rots, 2022), and actualistic taphonomic experiments, performed under natural or uncontrolled outdoor conditions, where only limited parameters such as sediment type and burial depth can be standardized. The latter approach, though less predictable, provides a critical opportunity to examine how multiple environmental factors interact to shape residue transformation under realistic conditions. By burying stone tools with known adhesive mixtures under such actualistic taphonomic conditions, it becomes possible to observe how different environments leave distinct molecular fingerprints, track the pace of degradation, and identify the spectral transformations most diagnostic of taphonomic change. This study builds on prior work showing the macroscopic persistence of resin-beeswax adhesives after 3 years of burial (Cnuts and Rots, 2024). Here, we focus explicitly on the chemical dimension of that persistence, addressing how quickly and in what ways the FTIR spectra of these adhesives diverge from their pristine states. Our aim is to determine whether FTIR can resolve environment-associated degradation signatures, and, by extension, strengthen the interpretive framework for archaeological residues.

2 Materials and methods

2.1 Materials

The specimens analyzed in this study derive from a wider experimental program that included 1-year and 3-year surface exposure experiments alongside a 3-year burial experiment, designed to evaluate the preservation potential of residues on stone tools under temperate weathering and depositional contexts (Cnuts and Rots, 2024). The broader research framework manipulated behavioral and environmental parameters while maintaining experimental controls to better understand residue taphonomy. Across the original experiment, key variables including raw material, adhesive recipe, and use duration were held constant, while worked material, depositional environment, and exposure conditions were systematically varied to evaluate their influence on residue survival.

All tools were knapped out of Harmignies flint by an experienced primitive technologist (C. Lepers, TraceoLab, Belgium) and hafted using a mixture of 70% spruce resin (*Picea abies*) and 30% beeswax, some being reinforced with leather bindings. Tools were used for a minimum of 20 min prior to deposition to ensure sufficient residue accumulation, with experimental activities involving processing of hardwood, soft plants, and dry or fresh bone. Following use, tools were immediately dehafted and subjected to their respective post-depositional conditions, positioned with the ventral side facing downward in contact with the sediment. In the 3-year burial experiment, twenty-six tools were buried for 3 years at a depth of 20 cm below the surface (Cnuts and Rots, 2024). Burial was conducted in four distinct environments: sand (Lommel), loess (Val-Meer), forest soils (Rochefort), and cave sediments (Scladina). Key environmental parameters for each burial context are summarized in Table 2.

While the initial project examined both surface weathering and burial scenarios, the present study draws primarily on the 3-year burial experiment. One specimen from the 3-year surface exposure experiment was also included to provide an additional point of comparison across post-depositional environments.

From the larger experimental assemblage presented in Cnuts and Rots (2024) and briefly described above, nine pieces were selected for detailed FTIR analysis. Selection was based on (i) known presence of an adhering spruce-beeswax adhesive; (ii) coverage of all depositional environments; and (iii) access to samples for testing. It is important to explicitly note that this study is based on a small sample size (n = 9), and though it prioritizes comparability across contexts, an inherent bias is introduced by the small dataset. We therefore treat all interpretations, particularly those that are environment-related, as exploratory. A summary of the selected specimens and their burial contexts are provided in Table 3. Pristine reference materials for beeswax, spruce resin, and a spruce resin-beeswax mixture were prepared and applied to flint flakes as well as glass slides to serve as unaltered samples for controlled comparison.

2.2 Methods

Prior to this study, the same set of experimental adhesives had been examined to document their macroscopic and microscopic preservation following burial. At recovery, residues were assessed for density, color change, fungal growth, and mineralization (Cnuts

TABLE 1 Proposed degradation products and their identification through diagnostic infrared spectral features.

Product/Phase	FTIR indicators (cm^{-1})	Possible degradation pathway observed in this dataset	Notes	References
Free fatty acids (beeswax), carboxylic acids	1700-1715 (C=O stretch); 1,465 & 730/720 (CH2 bending/scissoring)	Hydrolysis of ester-bound lipids	1710 peak	Evershed 1993; Derrick et al., 2000; Regert et al., 2001; Baales et al., 2017; Liu et al., 2019; Tanner and Lichtenberg-Kraag 2019; Duce et al., 2015; Čížová et al., 2019; Sano et al., 2019; Miłek et al., 2020; Kozowyk et al., 2025
Metal carboxylates (Ca/Mg soaps)	1,540-1,560 and 1,400-1,420 (asymmetric/symmetric COO- stretch); splitting of carboxylate bands; reduction or loss of 1710 peak	Reaction of free fatty acids with Ca/Mg	Characteristic broad asymmetric carboxylate peak ~1545cm^{-1}	Derrick et al., 2000; Ibrahim et al., 2005; Filopoulou et al., 2021; Nunziante-Cesaro and Lemorini 2012; Otero et al., 2014; La Nasa et al., 2018; Cotte et al., 2017; Lerchi et al. 2022; Russo et al., 2023; Tiomno-Tiomnova et al., 2020; Poli et al., 2024; Barannikov et al., 2024
Oxidized resin acids	1,680-1,695 (oxidized carboxyls); 1,270-1,285 (C-O); 880-890 (abietane skeleton); decrease of 1718 and 1,690 - > shift	Oxidation of diterpenoid resin acids	Oxidation produces abietadienic and dehydroabietic acids; peaks often broaden with oxidation	Derrick et al., 2000; Tappert et al., 2011; Sano et al., 2019; Helwig et al., 2014; Beltran 2016; Bruni and Guglielmi 2014; Piña-Torres et al., 2018; Saitta and Kaye 2025
Carbonates	1,420-1,480 (asymmetric CO3^2-), 870-880 (out-of-plane bend), 710-720 (in-plane-bend)	Mineral transfer	Can overlap with carboxylates and complicate identification	Farmer 1974; Weiner et al., 2002; Shillito et al., 2009; Lebon et al., 2010; Scaggion et al., 2024; Toffolo 2025
Silicates	Broad 1,000–1,100 (Si-O stretch); 780-800 (Si-O-Si symmetric); 460 (Si-O bend)	Substrate interference or mineral transfer	Typically featureless broad band; indicates mineral contamination	Farmer 1974; Socrates 2004; Shillito et al., 2009; Vahur et al., 2011; Tollan et al., 2019; Izzo et al., 2020; Kozowyk et al., 2025; Toffolo 2025
Oxalates	1,315-1,325 (C-O); 780-790 (C-C); 1,620-1,640 (COO-)	Biogenic surface films or oxidation products	May form due to contact with lichen or other living organisms	Monico et al., 2013; Ndzana et al., 2022
Hydroxylated phases/bound water	Broad 3,000–3,600 (OH stretch); 1,630-1,650 (H-O-H bend)	Moisture uptake; diagenetic hydration	Environmentally introduced hydration	Derrick et al. (2000); Socrates 2004
Aldehydes/ketones	1715-1740 (C=O stretch); 2,720-2,820 (aldehyde CH stretch); 1,230-1,260 (C-O)	Oxidation of unsaturated lipids and diterpenes	Can appear as a shoulder on the beeswax/resin ester carbonyl; oxidative aging	Evershed 1993; Regert, 2004; Socrates 2004; Shillito et al., 2009; Tappert et al., 2011; Vahur et al., 2011; Bruni and Guglielmi, 2014; Helwig et al., 2014; Favvas et al., 2015; Beltran et al., 2016; Martin-Ramos et al., 2018; Čížová et al. (2019)

TABLE 2 Environmental conditions of the 3-year burial experiment.

Experimental parameter	Rochefort	Lommel	Val-meer	Scladina
Number of tools (n)	8	8	5	5
Burial method	20 cm below surface	20 cm below surface	20 cm below surface	Buried in tube
Vegetation	Pine forest	Pine forest	Grasses	N/A
Sediment	Silt	Sand	Loess	Clay
Soil humidity	Humid	Humid	Humid	Dry
Soil pH	6.4	6.6	5.95	7.63
Bioturbation	Very high	High	Low	N/A
Biological activity	Very high	High	Low	N/A

TABLE 3 Overview of the experimental burial conditions for the nine selected samples. Additional details on the burial parameters are provided in Cnuts and Rots (2024) (SI).

Sample ID	Location	Burial context
49–12	Scladina	Cave, in soil
49–18	Lommel	Sand, in soil
49–26	Lommel	Sand, in soil
49–30	Rochefort	Forest, in soil
49–42	Rochefort	Forest, in soil
49–44	Rochefort	Forest, on surface
49–48	Val-meer	Loess, in soil
49–52	Rochefort	Forest, in soil
49–56	Lommel	Sand, in soil

and Rots, 2024). Initial inspections were performed under optical microscopy, with subsequent high-magnification analysis carried out using scanning electron microscopy (SEM). Energy dispersive X-ray spectroscopy (EDS) provided preliminary information on elemental composition and mineral incorporation (Cnuts and Rots, 2024). These earlier analyses revealed the persistence of resin-beeswax adhesives at the macroscopic scale despite visible signs of surface alteration, forming the basis for the present study's focus on their chemical evolution through reflectance-mode FTIR.

During this study, FTIR spectra were collected in reflectance mode using a Bruker LUMOS II microscope, equipped with an internal ceramic source, a zinc selenide (ZnSe) beamsplitter and a thermoelectrically cooled mercury-cadmium-telluride (TE-MCT) detector with a spectral range of 4,000–650 cm^{-1}, operating through the Bruker OPUS software. Given the limited spectral range of our measurements, bands approaching the lower wavenumber limit are more difficult to interpret, and any assignments in this region are made cautiously. Background scans were collected on gold, and spectral resolution was maintained at 2 cm^{-1}. Scan parameters were standardized at 400 co-added scans per spectrum, with aperture ranging between 100 × 100 µm to 250 × 250 µm depending on residue spot size and surface topography. The use of FTIR microscopy allowed for precise targeting of residues on lithic surfaces, minimizing spectral interference from surrounding mineral phases and enabling a higher spatial accuracy of band assignment. The analytical approach applied here was informed by previous FTIR studies of archaeological and experimental residues, which demonstrated the value of reflectance-mode measurements for characterizing organic components on lithic surfaces (Prinsloo et al., 2014; Monnier et al., 2017; Croft et al., 2016; Croft, 2021). It also draws on established practices in micro-FTIR analysis more broadly (Derrick et al., 2000; Socrates, 2004; Stuart 2021; De Haseth and Griffiths, 2007), while adapting acquisition parameters to the specific requirements of residue morphology and surface heterogeneity. Multiple spectra were collected from each specimen, ranging between a minimum of three and a maximum of eight points, targeting visually distinct regions of the adhesive surface to gather holistic representative spectra. Where present, areas showing variation in color, texture, or mineral overgrowth were specifically analyzed to capture the heterogeneity of residue surfaces and its potential impact on resulting FTIR spectra (Figure 1). Both dorsal and ventral faces were examined when residues were preserved, although in most cases adhesive material was concentrated on ventral surfaces.

Spectra were processed in Peak Spectroscopy (Operant LLC) with the following steps: Kramers–Kronig transformation (KKT), auto-baseline correction (function fit method, quadratic correction order, data normalized to a zero baseline minimum), CO_2 band removal, and smoothing with a 17-point Savitzky-Golay (SG) filter (quadratic/cubic algorithm). The KKT was applied to convert raw reflectance spectra into absorption-like profiles, allowing direct comparison with existing transmission-based reference data. This step is particularly critical given the current lack of large, standardized reference datasets of reflectance-mode spectra, especially for complex archaeological residues. Additionally, applying KKT minimizes distortions caused by refractive index effects and surface scattering, thereby enhancing band positions and relative intensities for more accurate material identification (Daher et al., 2013; Prinsloo et al., 2014). Pristine reference adhesives and base materials were prepared, processed, and analyzed under identical conditions for direct comparison, and additional library standards within the Helen and Martin Kimmel Center for Archaeological Science Infrared Spectra Library (Weizmann Institute of Science) were consulted as needed. Peak positions were recorded for each individual point in each sample to capture local

10.3389/fmats.2026.1764261

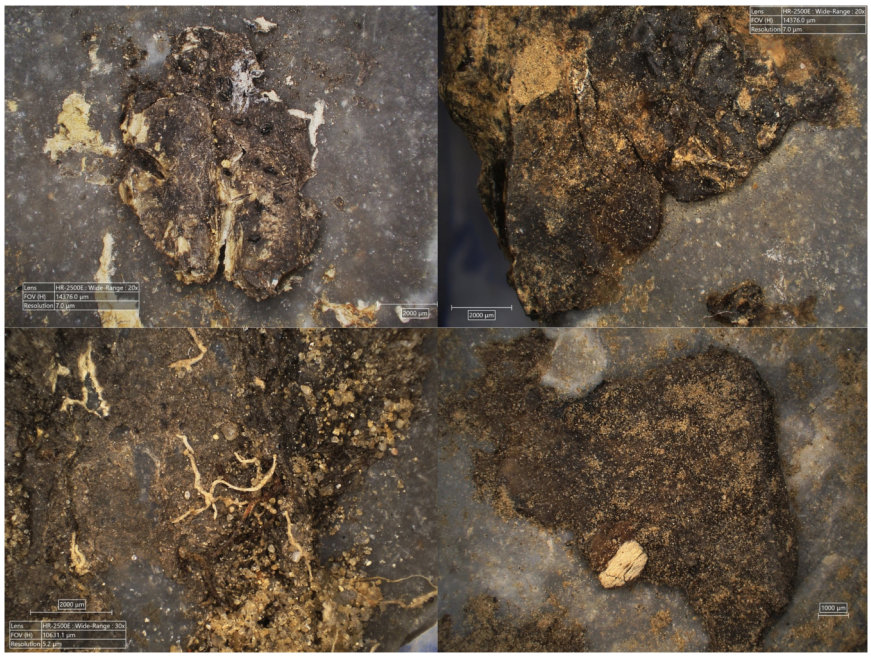

FIGURE 1
Examples of residue surface preservation across experimental and burial contexts, illustrating variation in texture, integrity, and visible alteration. Top left: 49-12; top right: 49-42; bottom left: 49-56; bottom right: 49-48.

compositional variability and identify diagnostic peaks. Recorded peaks were identified manually and confirmed with automatic peak-picking features in Peak Spectroscopy, measuring peaks by their maximum and using cubic splines to locate them precisely.

As part of the visual comparison process, an averaged spectrum was generated for each specimen by combining spectra from all measurement points into a single representative spectrum using processed spectral data files. For comparative purposes, synthetic spectra were also produced by averaging real spectra of materials believed to contribute to the observed signals. The averaged spectra were then used in conjunction with the individual spectra to facilitate visual comparison with reference materials. This approach preserved the inherent heterogeneity within each sample while providing a clearer representation of overall spectral trends, allowing entire specimens to be compared more effectively to both experimentally acquired references and synthetic composite spectra. While synthetic spectra based on linear averaging provide a useful heuristic for visual comparison, infrared mixtures often exhibit non-linear behavior due to scattering, matrix effects, and chemical interactions among components (Daher et al., 2013; Daher and Bellot-Gurlet, 2013; Izzo et al., 2021; Russo et al., 2023). As such, these composite spectra are interpreted qualitatively rather than quantitatively, serving to assess overall spectral comparability and highlight possible source contributions rather than to model precise compositional proportions. All spectral images were produced in Peak Spectroscopy.

A preliminary principal component analysis (PCA) was undertaken as a pilot exercise to assess whether reflectance-mode FTIR data might reveal early-stage patterns of residue degradation across burial environments or preservation states. Both raw and KKT-transformed datasets were examined under a variety of preprocessing strategies including derivatives, standard normal variate (SNV), generalized least squares weighting (GLSW), and mean-centering, with the aim of testing methodological sensitivity rather than generating definitive classifications. Final models for raw data included mean centering, while final KKT-transformed models included application of a first derivative, GLSW (0.05), and mean-centering. The same model was also applied to a dataset of averaged spectra for comparison purposes.

To assess the influence of specimen orientation during analysis, orientation tests were conducted on four pieces: 49-12, 49-44, 49-48, and 49-52. For each piece, two distinct points were selected and scanned four times each, with the sample rotated by 90° clockwise between scans. This design provided a controlled assessment of whether orientation effects, such as changes in reflectance angle, surface heterogeneity, or anisotropy of the residue, might influence the reproducibility of spectral outputs (Van Nimmen et al., 2008; Mercurio et al., 2011; Belbachir et al., 2011; Izzo et al., 2020). Orientation testing was included to evaluate whether rotation-related artifacts might explain some of the intra-sample variability observed elsewhere in the dataset.

3 Results

3.1 Spectral trends and material preservation

The spectra generated on these materials revealed both preserved organic signatures derived from the base ingredients

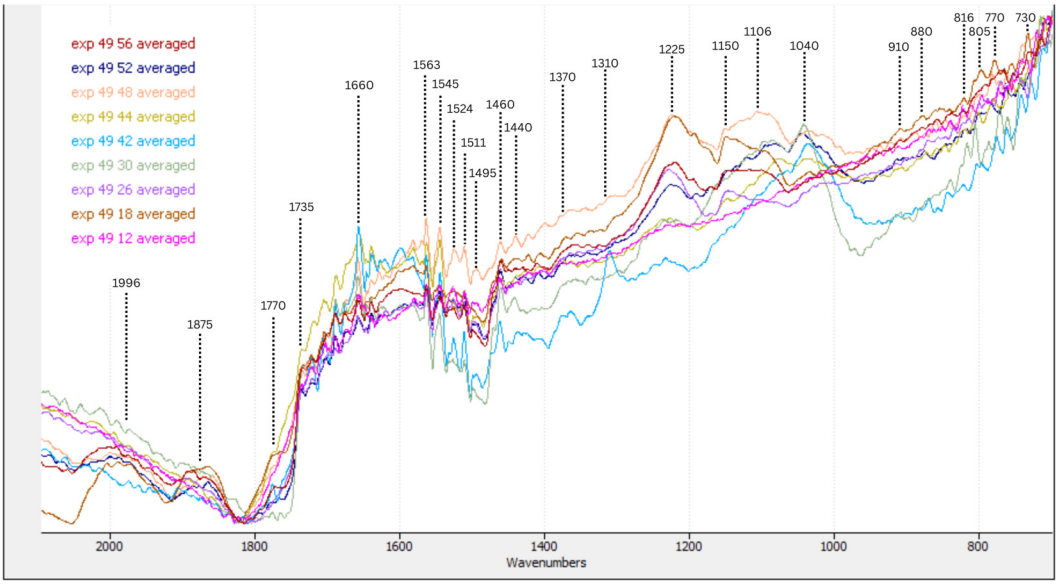

FIGURE 2
Averaged FTIR spectra of the experimental adhesives, highlighting the most prominent peaks within the fingerprint region.

as well as clear evidence of post-depositional alteration across the nine specimens analyzed. The applied multi-point acquisition strategy followed by spectral averaging allowed us to characterize the general preservation state of each specimen without concern for the possibility of intra-sample heterogeneity being a significant bias, while also highlighting localized variability that might otherwise be overlooked (Figure 2). The resulting spectra therefore capture both the robustness of certain chemical markers and the inconsistency of degradation processes and post-depositional influences across contexts and even across a single artifact.

To summarize these observations, Table 4 presents an overview of the main spectral indicators recorded across all specimens, including the presence or absence of key molecular markers (e.g., esters, carboxylates, aromatics, carbonates) and other relevant taphonomic features. More detailed diagnostic peak tables are provided in the (Supplementary Table S1). A second table (Table 5) lists peaks excluded from the wider interpretation and assigns likely sources for each.

The averaged spectra reveal consistent patterns across specimens while highlighting meaningful variation linked to environmental contexts. The cave sample (Scladina, 49-12) exhibited the strongest retention of organic markers, including well-defined CH_2, ester, and aromatic peaks. Forest-soil specimens (Rochefort series) also preserved major adhesive components but showed variable carbonate and silicate interference. Adhesives recovered from sandy contexts (Lommel series) displayed weaker hydrocarbon and ester bands, partial masking of the beeswax doublet, and stronger carbonate signals. The loessic specimen (Val Meer, 49-48) retained relatively strong organic signals despite notable silicate background influence. These differences collectively reinforce that preservation quality and degradation signatures correlate closely with sediment type and depositional environment; cave contexts favor chemical stability, whereas open-air sandy deposits promote oxidative alteration, with loessic and forest settings occupying intermediate positions.

A consistent trend across the dataset is the persistence of the long-chain hydrocarbon framework in beeswax (Edwards et al., 1996; Regert, 2004; Baales et al., 2017; Čížová et al., 2019; Tanner and Lichtenberg-Kraag, 2019; Miłek et al., 2020). The CH_2 asymmetric stretching vibration (~2,918 cm^{-1}), CH_2 symmetric stretch (~2,849 cm^{-1}), CH_2 scissor (~1,475–1,458), CH_3 δ (~1,375), and the ester C=O stretch (~1735 cm^{-1}) appear in nearly all samples, although their intensity can be masked relative to pristine reference spectra (Baales et al., 2017; Čížová et al., 2019; Mazurek et al., 2019; Tanner and Lichtenberg-Kraag, 2019; Miłek et al., 2020; Bertelli et al., 2023). In some cases, the ester band is reduced or partially obscured by emerging carboxylate signals. By contrast, the CH_2 stretching bands remain present, suggesting relative chemical stability of the wax backbone compared to the ester linkages. These bands provide the clearest throughline across the assemblage, demonstrating that even after 3 years of burial in diverse environments, the functional groups of beeswax remain largely diagnostic. While CH_2 stretching bands are not unique to beeswax, their sharpness, narrow separation, and nearly equal intensity, together with more diagnostic features such as the 1735 cm^{-1} ester band and in some cases the 730/720 cm^{-1} rocking doublet, enable more reliable identification when assessed in combination. Although some of these aliphatic stretches fall outside of the formal fingerprint region and are therefore less compound-specific, they remain among the most resilient features. The CH_2 rocking doublet, when present, further supports the identification of beeswax (Baales et al., 2017; Miłek et al., 2020). However, its absence in several sandy and surface samples does not necessarily indicate the chemical loss of wax components. Instead, it likely reflects either spectral masking by carbonate phases or the disruption of molecular ordering through oxidative and physical weathering processes. In

TABLE 4 Diagnostic phases identified for primary interpretations. Legend: ++ = strong/clearly defined; + = moderate; +/– = weak/ambiguous; - = absent or not detected.

Specimen	Beeswax ester C=O (~1735 cm^{-1})	Resin acidic/oxidized C=O (~1720–1700)	Beeswax aliphatic (CH_2 sciss. ~1,475–1,458; CH_3 δ ~1,375)	Carboxylates (~1,560/ 1,410 cm^{-1})	Resin aromatic ring (~1,515 cm^{-1})	Carbonate (v_2 ~875, v4 ~712 cm^{-1})	Beeswax rocking doublet (~730/720 cm^{-1})	Silicate (~1250-1000 cm^{-1})	CH_2 bands (2,920/2, 850 cm^{-1})	Notable absences/ overprints	Overall preservation
49–12	++	+	+	++	++	++	++	+	++	Minor carbonate crust, organics clearly defined	Good
49–18	+	++	+	++	+/–	+	+/–	+	+	Aromatic weak, C=O broadened (oxidation)	Moderate
49–26	++	++	+/–	++	+	++	+	+	++	Strong carbonate v_2, partial silicate masking	Moderate
49–30	++	++	+	++	++	+	++	+	++	Mild shift of C=O (oxidation), minor masking	Good
49–42	++	++	+	++	++	+	++	+	++	Slight v4/CH_2 overlap, otherwise intact	Good
49–44	+/–	+/–	+/–	+	+/–	++	-	++	+/–	Beeswax doublet absent, strong carbonate baseline	Poor-moderate
49–48	++	++	+/–	++	++	++	++	++	++	Stong Si-O background, minor oxidation	Good
49–52	++	++	+	++	+/–	++	++	++	++	Carbonate overprint, overlapping CH_2/COO^- bands	Good
49–56	+	+	+/–	++	+/–	++	+/–	++	+/–	Aromatic weak, strong carbonate and oxidation masking	Moderate-poor

10.3389/fmats.2026.1764261

TABLE 5 Peaks and bands excluded from the primary interpretations and their likely sources.

Wavenumber(s)	Likely source	Notes
>1850cm^{-1}	Combination/Overtone bands of carbonyls, quartz, or carbonates	Combination/Overtones
1775-1750cm^{-1}	Weak high-frequency carbonyl shoulders; instrument/Interface artifacts	May be linked to adhesive signals
1655-1630cm^{-1}	H-O-H bending of absorbed/Bound water; clay OH deformation	Possible but unlikely protein/Amide
1598-1580cm^{-1}	Aromatic conjugation and COO- broadening; composite/Overlapping	Mentioned as non-diagnostic shoulders
1540-1480cm^{-1}	Resin/Carboxylate composite region; peak multiplicity, not interpreted individually	Primary aromatic band (~1515 cm^{-1}) used
1475-1375cm^{-1}	CH_2 bending and COO^- symmetric stretch overlap	Treated as composite signals, complex cluster
1310-1300cm^{-1}	Resin oxidation or clay overtones, possible oxalate	Ambiguous
1250-1000cm^{-1}	Silicate framework vibrations	Substrate masking
920-800cm^{-1}	Carbonate overtones and silicate mixtures	Sediment masking
780-720cm^{-1}	CH_2 rocking and carbonate v_4 interference	Used cautiously

this respect, the doublet provides a useful qualitative indicator of preservation state rather than a strict criterion for beeswax presence. Inclusion of the 1,475–1,375 cm^{-1} window (CH_2 scissoring and CH_3 deformation of aliphatic, non-aromatic compounds) offers complementary support for beeswax where unmasked; however, its diagnostic expression is frequently diminished by overlap with carbonate v_3 (~1,470–1,420 cm^{-1}) and carboxylate COO^- (~1,415–1,400 cm^{-1}). Consequently, the persistence argument rests primarily on the CH_2 stretching pair (2,920/2,850 cm^{-1}), the ester C=O (~1735 cm^{-1}), and, where not obscured, the rocking doublet (730/720 cm^{-1}). Weak or absent bands in the 1,475–1,375 cm^{-1}, 1,170 cm^{-1}, and 956 cm^{-1} regions were thus interpreted as probable masking rather than definitive loss or absence of beeswax.

This pattern carries notable archaeological implications. Because beeswax's long-chain hydrocarbons are among the most chemically stable components observed here, their persistence strongly suggests that when beeswax is present, it is likely to remain detectable even after prolonged burial. Conversely, the complete absence of beeswax markers in a residue that otherwise retains organic signals is unlikely to result solely from degradation and may therefore indicate that beeswax was never originally present in the mixture. Such interpretive stability reinforces the value of CH_2 and CH_3 bands as reliable indicators of wax inclusion even in highly altered archaeological contexts.

By contrast, spruce resin markers are far more labile and easily obscured. Aromatic C=C stretching modes (~1,518–1,512 cm^{-1}) and acidic C=O bands (~1720–1700 cm^{-1}) are variably reduced, split, or broadened depending on burial environment (Regert, 2004; Tappert et al., 2011; Bruni and Guglielmi, 2014; Helwig et al., 2014; Beltran, 2016; Martín Ramos et al., 2018; Schmidt and Koch, 2024). Across all specimens, we detect carboxylate features at ~1,563/1,544 cm^{-1} (COO^- asymmetric) and ~1,415–1,400 cm^{-1} (COO^- symmetric), interpreted as a carboxylate doublet consistent with soap-salt formation, while noting potential overlap with carbonate v_3 and reflectance-related distortions (Palacios and Monhemius, 2001; Ibrahim et al., 2005; Otero et al., 2014; Filopoulou et al., 2021; Izzo et al., 2021; Russo et al., 2023). The doublet is most pronounced, often approaching or even surpassing the ester C=O at ~1735 cm^{-1}, in samples 49-12, 49-18, 49-26, 49-42, 49-44, 49-48, and 49-52, and is present but weaker or partially masked in 49–30 and 49-56, suggesting a shift from intact esters toward carboxylate salts (Palacios and Monhemius, 2001; Ibrahim et al., 2005; Otero et al., 2014; Cotte et al., 2017; La Nasa et al., 2018; Filopoulou et al., 2021; Izzo et al., 2021; Barannikov et al., 2024; Russo et al., 2023; Thanaa, 2024; Poli et al., 2024). This pattern may be consistent with saponification, but such an attribution should be made cautiously here, as overlapping contributions from environmental carbonates or root-derived acids cannot be excluded.

Notably, the surface specimen (49-44) displays strong carboxylate signals despite less intrusive sediment contact. This pattern may reflect photo-oxidative and oxidative weathering at exposed surfaces; UV, oxygen, and humidity can break ester bonds to yield free fatty acids leading to an increase in carbonyl/carboxyl bands, which can then form metal carboxylates upon contact with rain-delivered or airborne Ca/Mg particulates, producing a COO^- doublet similar to that seen after burial (La Nasa et al., 2018). Similar transformations have been described in aging waxes and heritage coatings, where oxidative degradation or hydrolysis alone can produce distinct COO^- signals (La Nasa et al., 2018; Izzo et al., 2021; Russo et al., 2023). Thus, surface exposure can converge chemically with burial transformation processes, with both pathways leading to prominent carboxylate signatures, even though the dominant drivers are significantly different.

Averaged spectra generated from all measurement points per specimen provided representative profiles that could be directly compared to references of beeswax and spruce resin (Daher et al., 2013; Baales et al., 2017; Monnier et al., 2017). Importantly, the averaged spectra synthesize whole-specimen trends while preserving intra-sample heterogeneity captured by point-wise analysis, enabling comparisons at both local (point) and global (specimen) scales. Across series (49-12, 49-18, 49-26, 49-30, 49-42, 49-44, 49-48, 49-52, 49-56), the averaged profiles consistently retained beeswax-derived CH_2 stretches (~2,950–2,850 cm^{-1}) while showing specimen-specific variation in the carbonyl and carboxylate region (~1735–1,400 cm^{-1}), where spruce-resin signals and carboxylates interact. In several specimens (e.g., 49-12, 49-30, 49-42) the averaged carbonyl envelope aligns more closely with

spruce resin, whereas others (e.g., 49-18, 49-44, 49-56) emphasize stronger aliphatic bands akin to beeswax.

3.2 Environmental and contextual trends

Other spectral changes highlight the role of environmental inputs. Carbonate peaks at ~880–870 cm^{-1} (ν_2) and ~722–703 cm^{-1} (ν_4) (Weiner et al., 2002; Lebon et al., 2010; Toffolo, 2025) appear clearly in the cave sample, often coinciding with whitish crusts visible macroscopically. Higher-frequency carbonate-related bands in the ~1,470–1,420 cm^{-1} region are also observed, likely overlapping with CH_2 scissoring vibrations and complicating confident interpretation (Weiner et al., 2002; Lebon et al., 2010; Scaggion et al., 2024; Toffolo, 2025).

The loess sample, by contrast, still shows carbonate peaks but to a weaker extent. The acidic conditions here are expected to accelerate hydrolysis and oxidation of the resin-beeswax mixture, promoting cleavage of the ester linkages and oxidation of the resin acids. These processes correspond to the attenuated ester C=O (~1735 cm^{-1}) and the emergence of carboxylate peaks (~1,560–1,415 cm^{-1}) in this sample, consistent with partial conversion of esters into metal carboxylates and oxidized acids. Despite the acidic environment, preservation of diagnostic markers of the organic residue was still considered good.

Alternatively, sandy contexts show more pronounced OH-stretch broadening between 3,600–3,200 cm^{-1}, consistent with oxidation, hydration, and fungal activity (Child, 1995 Teacă et al., 2013; Huisman et al., 2017; Łucejko et al., 2018). In several samples, SEM and digital microscopy imaging corroborate these patterns (Figure 3) by documenting fungal overgrowth penetrating overlaying residues, while EDS detects calcium and magnesium in crusted regions suggesting both microbial and mineral overprints (Cnuts and Rots, 2018; Michel et al., 2019; Hayes and Rots, 2019; Hayes et al., 2019; Cnuts and Rots, 2024).

Weak but broad recurrent features are observed between ~2050 and 1800 cm^{-1} in samples 49-18, 49-30, 49-48, 49-52, and 49-56. These bands are unlikely to correspond to fundamental vibrational modes but may instead represent overtone or combination bands, such as from mineral phases, which can be accentuated under reflectance conditions (Farmer, 1974; Socrates, 2004; Daher et al., 2013; Prinsloo et al., 2014; Tollan et al., 2019). Their reproducibility across these samples suggests that they are not random noise, and that they are likely an environmental product; however, given their weak intensity, broad width, and ambiguous origin, they are interpreted with caution. Considering the environmental contexts and visual characteristics of the analyzed points, the most plausible explanation is that these absorptions correspond to overtone or combination bands of quartz or other silicate or carbonate minerals within the substrate (Tollan et al., 2019; Izzo et al., 2020). Such mineral overtones are known to occur in this spectral region under reflectance conditions and may variably influence the baseline or produce subtle peaks and shoulders depending on surface composition and orientation (Farmer, 1974; Tollan et al., 2019).

In addition to mineral and microbial overprinting, some spectral features could plausibly reflect contributions from plant root activity, particularly in forest and loess contexts where root density is typically high (Tjelldén et al., 2015; Ortega-Villamagua et al., 2020; Ma et al., 2022; Ndzana et al., 2022). In a few specimens, notably 49-30 (points 1-2) and 49-42 (points 2-5), weak but somewhat broad bands appear in the 1,030–1,020 cm^{-1} region alongside enhanced OH stretches (3,600–3,200 cm^{-1}). While these can be consistent with silicate inputs, the possibility of overlapping signals from root exudates such as cellulose, hemicellulose, or lignin derivatives cannot be excluded (Boeriu er al. 2004; Chambre and Dochia, 2021). Some forest samples exhibit strong localized carboxylate doublets paired with faint shoulders near 1,320–1,310 cm^{-1}, a range where oxalates may absorb (Ström et al., 2001; Tjelldén et al., 2015; Ortega-Villamagua et al., 2020; Ma et al., 2022; Ndzana et al., 2022). Though this is not conclusive, it does raise the possibility that root-associated acids and oxalates may have contributed to localized residue alterations. However, features that might initially resemble oxalate-related absorptions are not strongly supported here: the diagnostic oxalate triplet (1,620-1,640, 1,315-1,325, and 780–790 cm^{-1}) is absent or very weak across the dataset. This indicates that oxalate formation did not occur to a measurable degree and that root- or fungus-derived oxalic acid did not substantially influence residue chemistry. Instead, the shoulders present in the ~1,320 cm^{-1} region are more plausibly attributed to carbonate-carboxylate overlap or

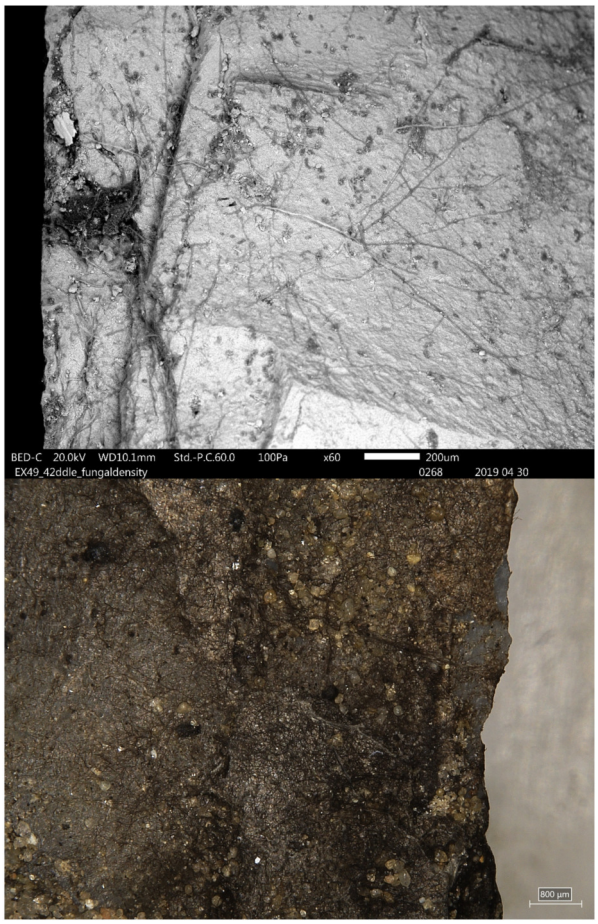

FIGURE 3
SEM image of 49–42 (top) and Hirox image of 49–26 (bottom) showing evidence of fungal activity on adhesive surfaces, including hyphal imprints and localized surface degradation.

reflectance-related distortions rather than discrete oxalate phases. No direct visual evidence of root penetration was observed during SEM examination, but the spectral variability across points within single specimens suggests that root- and fungus-related processes may represent one additional microenvironmental factor influencing residue transformation.

In several specimens (such as 49-12 point 1-2, 49-18 points 2-5 and 49-44 points 1-6), carbonate fundamentals (ν_2 at ~880–870 cm^{-1} and ν_4 at ~722–703 cm^{-1}) co-occur with strong carboxylate doublets (~1,560/1,544 and ~1,415 cm^{-1}) (Weiner et al., 2002; Lebon et al., 2010; Scaggion et al., 2024; Toffolo, 2025). This spatial and spectral overlap suggests that the chemical progression from ester hydrolysis to carboxylate salt formation is closely tied to sediment mineral input. SEM/EDS observations from Cnuts and Rots (2024) demonstrate Ca- and Mg-rich crusts in association with fungal growth, but root-derived processes may also contribute. Roots release organic acids including oxalate, citrate, and malate, which react with carbonate minerals in the soil, leading to their dissolution and the subsequent release of divalent cations such as calcium and magnesium into porewater (Karkanas et al., 2000; Weiner et al., 2002; Ström et al., 2001; Karkanas, 2010; Lebon et al., 2010; Tjelldén et al., 2015; Ortega-Villamagua et al., 2020; Ma et al., 2022; Ndzana et al., 2022; Scaggion et al., 2024), providing exogenous Ca/Mg that can drive carboxylate salt formation from adhesive acids (Otero et al., 2014; Filopoulou et al., 2021), prime for forming the metal carboxylates detected here. In effect, the carboxylate signatures may not only represent endogenous saponification but also root-mediated mobilization of mineral cations that accelerate metal-carboxylate formation (Karkanas et al., 2000; Ström et al., 2001; Weiner et al., 2002; Karkanas, 2010; Lebon et al., 2010; Ndzana et al., 2022).

Collectively, these patterns illustrate how carbonate-rich, buffered cave contexts promote stabilization and mineral encapsulation, whereas acidic, open-air environments foster more hydrolysis, oxidation, and leaching. While both environments ultimately yield carboxylate formation, their formation mechanisms and extent differ. In cave settings, the alkaline and carbonate-buffered conditions promote ion exchange and saponification reactions between fatty acids liberated by ester hydrolysis and divalent cations (Ca, Mg) derived from local carbonates. This pathway stabilizes residues through the precipitation of metal carboxylates, contributing to partial encapsulation of organic matter. In open-air contexts, by contrast, the acidic, weakly buffered soils favor acid-catalyzed hydrolysis and microbial oxidation, generating free organic acids that readily interact with the transiently available cations from water movement. Because these environments lack sustained buffering, reactions proceed under fluctuating moisture, pH, and oxygenation conditions, leading to more variable and less mineral-stabilized residues. Despite these contrasting pathways, both settings converge somewhat through the formation of carboxylate salts, albeit through distinct acidic versus alkaline mechanisms of degradation.

3.3 Multivariate results

Given the small sample size (n = 9), PCA was explored as a pilot approach to evaluate whether the current data might capture environment-related patterning. Because of this, we do not claim accurate classification or prediction, and present these results with caution as a means of probing the potential of multivariate analysis to data of this type.

When conducted on the raw, mean-centered spectra, the first two components accounted for roughly 90% of total variance (PC1 = 59%, PC2 = 25%). Moderate clustering by depositional environment was observed, with forest and sand samples occupying distinct regions of the score plot, whereas cave and loess specimens plotted closer to the origin, suggesting lower within-group variability and weaker environmental signal contrast (Figure 4). Despite this, there is still significant overlap between groups. The strong influence of low-frequency mineral bands likely contributed to the separation of carbonate-encrusted samples, indicating that matrix composition exerts a major control on spectral variance.

Analysis of the KKT-transformed spectra using a first derivative, GLSW (0.05) decluttering, and mean center preprocessing produced the most defined results. This configuration accounted for over 50% of total variance across the first three components (PC1 = 21.9%, PC2 = 17.5%, PC3 = 14.3%) and generated distinct clusters for each environmental type represented. Forest and sand specimens formed compact, internally consistent groups, while cave and loess samples remained tightly grouped and separated, reflecting compositional variability. The derivative preprocessing enhanced subtle signals, while GLSW minimized baseline curvature and reflectance-related noise, allowing environmentally conditioned differences in residue preservation to emerge.

PCA of averaged specimen spectra yielded similarly well-defined clusters despite reduced overall variance. Averaging produced more compact groupings by minimizing point-level heterogeneity, yet retained clear environmental separation, with sand, forest, cave and loess samples again trending apart. This demonstrates that spectral averaging preserves diagnostic variance while suppressing localized noise, providing a robust means of comparing specimen-level compositional trends across depositional contexts.

Together, these results indicate that depositional environment exerts a detectable influence on the spectral signatures of residues, observable in both averaged and preprocessed datasets. The consistency of cluster separation across independent treatments suggests that the observed structure reflects genuine compositional and preservation-related differences rather than artifacts of preprocessing. Nevertheless, given the small sample size (n = 9) and the sensitivity of clustering to data treatment, these outcomes should be considered exploratory, providing a propitious foundation for future multivariate analyses on expanded experimental and archaeological datasets.

3.4 Orientation effects

Orientation series collected on four specimens (49-12, Scladina, cave; 49-44, Rochefort, forest; 49-48, Val-Meer, loess; and 49-56, Lommel, sand) demonstrate that peak positions are generally invariant within measurement noise across rotations. In all cases, the principal bands remain fixed at ~2,918 and ~2,849 cm^{-1} (beeswax CH_2 stretches), ~1735–1710 cm^{-1} (ester/acid C=O), ~1,565–1,543 and ~1,416–1,408 cm^{-1} (COO^- asymmetric/symmetric), and ~874–860 and ~722–703 cm^{-1} (carbonate ν_2/ν_4). For the cave

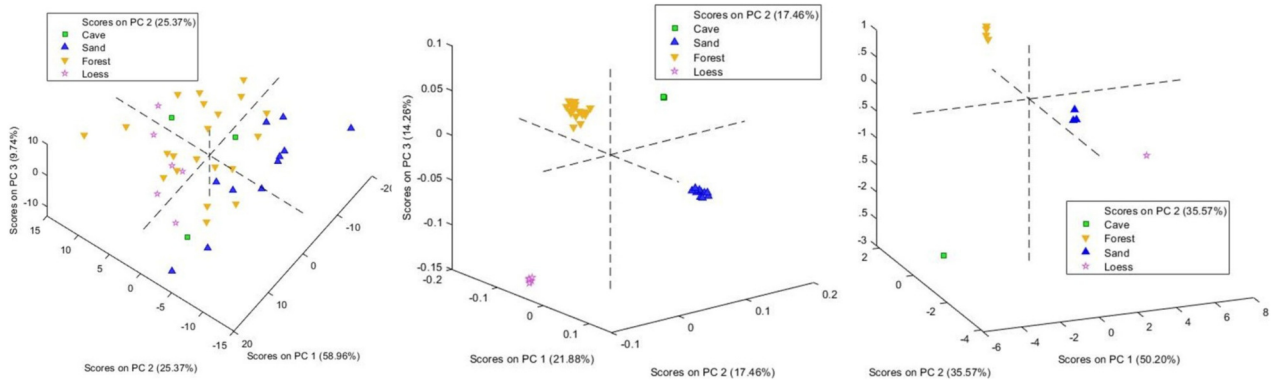

FIGURE 4
Multivariate analysis of the spectral dataset. Left: PCA of raw spectra. Middle: PCA of KKT-transformed first-derivative spectra (GLSW, mean-centered). Right: PCA of averaged spectra.

sample (49-12), both tested points show close overlay in wavenumber with only baseline and amplitude shifts; no diagnostic bands appear or disappear between rotations. The forest sample (49-44) retains consistent COO^- doublets and carbonate fundamentals in every orientation, with modest intensity differences most evident in the 3,600–3,200 cm^{-1} OH region and the 1,470–1,420 cm^{-1} window. The loess sample (49-48) exhibits nearly indistinguishable band positions across rotations, with small baseline tilts but stable CH_2, C=O, COO^-, and carbonate maxima. The sand sample (49-56) shows tight agreement at point 6, whereas at point 7 three rotations overlay strongly while one spectrum displays suppressed organic intensities and enhanced curvature; this outlier likely reflects local surface heterogeneity or scattering caused by anisotropy. Collectively, these spectra indicate that under our acquisition conditions, rotation did not create, shift, or erase diagnostic bands; variability is dominated by baseline and relative-amplitude changes attributable to reflectance geometry and residue micro-topography. Orientation-related artifacts therefore cannot account for the intra-sample chemical variability documented elsewhere in the dataset, and the assignments of wax CH_2, ester C=O, COO^- doublets, and carbonate ν_2/ν_4 are robust to rotation.

4 Discussion

4.1 General degradation patterns and methodological considerations

The results of this study highlight both the resilience and fragility of mixed spruce-beeswax adhesives under varied burial conditions, while also underscoring the complexity of interpreting FTIR spectra from degraded organic residues. Certain trends emerge consistently, such as the persistence of CH_2 stretching modes and the recurring appearance of carboxylate peaks, yet these signatures are not universally distributed across the sample nor even across certain burial contexts, cautioning against overly rigid interpretive frameworks. Instead, the data suggests that degradation pathways described here are probabilistic rather than deterministic, shaped by the interplay of chemical, mineral, and biological feedback factors related to individual microenvironment (Wadley et al., 2004; Haslam, 2004; Haslam, 2006; Monnier et al., 2013; Rots et al., 2016; Pedergnana et al., 2016; Pedergnana, 2020; Zurro and Gadekar, 2024).

The orientation tests indicate that spectral variability linked to specimen rotation is minimal. While slight changes in baseline intensity were observed, these did not impact peak presence or assignment. This finding is important for archaeological applications, where residue topography and mounting orientation can rarely be standardized, particularly when FTIR microscopy is not an option. The results suggest that, within the limits of this trial, reflectance-mode FTIR is robust against orientation artifacts in terms of chemical marker preservation. Nevertheless, caution is warranted, since only four specimens were tested here, and more complex residue morphologies may introduce stronger angular effects (Van Nimmen et al., 2008; Belbachir et al., 2011; Mercurio et al., 2011; Prinsloo et al., 2014; Tollan et al., 2019). Future work should expand orientation testing to a larger set of samples, including residues with high anisotropy or advanced mineral crusting, to ensure that orientation does not introduce subtle distortions in band intensity, shape, or presence.

Spectral averaging functioned as an interpretive bridge between point-level heterogeneity and whole-specimen comparisons (Daher et al., 2013; Monnier et al., 2017; Pedergnana and Ollé, 2018; Hayes and Rots, 2019; Hayes et al., 2019; Martín-Viveros and Ollé 2020). By integrating multiple measurement points into a representative profile, the approach emphasized dominant chemical trends without erasing localized variation. This dual scale of using averaged overlays against reference spectra (including the simulated composite spectrum) plus individual peak records improved confidence in identifying mixed organic signatures, in this case resin and wax, and in recognizing superimposed carboxylate features that may derive from degradation and mineral-organic interactions.

4.2 Chemical pathways in spruce resin-beeswax adhesives

One of the clearest chemical transformations observed is the emergence of metal carboxylate peaks, indicating possible

saponification and salt formation processes (Palacios and Monhemius, 2001; Ibrahim et al., 2005; Otero et al., 2014; Cotte et al., 2017; La Nasa et al., 2018; Filopoulou et al., 2021; Izzo et al., 2021; Barannikov et al., 2024; Thanaa, 2024; Poli et al., 2024). Across all samples, carboxylate peaks are present; the doublets are strongest in 49–12, 49-42, 49-44, 49-48, and 49-52, where carboxylate peaks equal or surpass the ester C=O stretch at ~1735 cm^{-1}, reflecting a pronounced chemical shift from intact esters toward hydrolyzed products (Otero et al., 2014; La Nasa et al., 2018; Filopoulou et al., 2021; Izzo et al., 2021; Russo et al., 2023). These bands typically appear as a diagnostic doublet, asymmetric COO^- (~1,560–1,540 cm^{-1}) and symmetric COO^- (~1,420–1,400 cm^{-1}), occasionally accompanied by subtle shoulders near ~1,310 cm^{-1} that may indicate secondary carboxylate coordination (Palacios and Monhemius, 2001; Ibrahim et al., 2005; Cotte et al., 2017; Izzo et al., 2021). However, this pattern is present but notably weaker or partially masked in 49–30 and 49-56, despite comparable burial histories. Such variability suggests that the formation of soap salts depends not only on burial matrix but also on micro-scale factors such as residue thickness, direct mineral contact, or microbial infiltration, and how these influence local interactions between residue and burial environment.

Within the resin-beeswax mixture, this transformation is most plausibly linked to the lipidic component of beeswax. Beeswax consists primarily of long-chain esters, hydrocarbons, and fatty acids, which readily undergo hydrolysis in the presence of moisture and catalytically active minerals. Subsequent reaction between liberated fatty acids and divalent cations (Ca, Mg) yields insoluble metal carboxylates, analogous to "soap" compounds (Filopoulou et al., 2021; Otero et al., 2014; Izzo et al., 2021; Russo et al., 2023). The resin fraction, dominated by terpenoid acids and alcohols, is less susceptible to true saponification but can undergo oxidation and secondary acid formation under aerobic, acidic, or microbially active conditions (Tappert et al., 2011; Gershenzon and Dudareva, 2007; Beltran, 2016; Bruni and Guglielmi, 2014; Martín Ramos et al., 2018; Schmidt and Koch, 2024). Some resin acids, such as abietic and dehydroabietic acid, are also capable of forming metal carboxylates under appropriate conditions, though this reaction proceeds more slowly and less completely than in lipidic systems (). Consequently, resin-derived carboxylates may contribute secondarily to the observed COO^- bands but are less likely to represent the primary source of these signals. This chemical division of vulnerability helps explain why carboxylate bands may appear even where resin-associated aromatic or ester signals have faded, suggesting selective alteration of the wax component.

Comparable transformations have been observed in other archaeological and experimental contexts. Studies of fat and adipocere residues demonstrate nearly identical carboxylate doublets in FTIR spectra, documenting the conversion of triglycerides into calcium and magnesium fatty acid salts under moist burial conditions (Solodenko et al., 2015; Venditti et al., 2019; Lerchi et al., 2022). However, the interpretation of such residues as true adipocere remains controversial, as similar metal carboxylates can form through multiple degradation pathways. Nevertheless, while those studies focus on animal fats rather than waxes and resins as is addressed here, both systems share common degradation pathways involving hydrolysis, ion exchange, and eventual stabilization as metal soaps. The COO^- doublet can, therefore, represent a reliable marker for terminal lipid alteration, regardless of the organic source. The presence of this same spectral pattern in the experimental adhesives points to a comparable endpoint for lipidic degradation under prolonged burial exposure.

We therefore emphasize that the observed carboxylate peaks represent a chemical state rather than a single reaction mechanism. Their presence signals advanced degradation but not necessarily the process by which it occurred. Likewise, their absence does not imply molecular stability; residues may lose their ester signatures through complete oxidation, volatilization, or dissolution without accumulating detectable salts. Collectively, these findings underscore the complexity of residue diagenesis in compound adhesives, where chemically distinct components such as lipidic wax and terpenoid resin follow divergent yet partially overlapping degradation trajectories that ultimately yield similar spectral outcomes.

4.3 Environmental mediation

From a mechanistic stance, the formation of carboxylate salts within these adhesive residues likely reflects an interplay of chemical hydrolysis, oxidation, microbial mediation, and cation availability, each of which operates differently across depositional environments. In carbonate-rich cave sediments, carboxylate formation is primarily driven by alkaline cation exchange, where Ca and Mg released from carbonate dissolution react with fatty acids to form stable metal soaps; this pathway favors stabilization and mineral encapsulation alongside carboxylate accumulation, often coinciding with limited oxidative alteration. In contrast, the loess environment represents an open-air system where carbonate buffering has been lost or weakened. Here, acid-catalyzed hydrolysis and oxidation dominate, driven by periodic wetting, microbial respiration, and organic acid inputs; limited cation supply permits strong but irregular carboxylate formation without the degree of mineral stabilization observed in caves. Sandy contexts are more chemically inert and poorly buffered, dominated by quartz with minimal capacity for ion retention. Carboxylate formation here occurs only episodically, during transient wet-dry cycles or following dust and porewater influxes that introduce trace Ca or Mg, producing spatially variable features. Forest soils amplify these same processes through high biotic activity. Organic acids from roots, fungi, and decomposing litter accelerate ester hydrolysis and oxidation while mobilizing ions from mineral and organic sources, yielding chemically similar but mechanistically distinct COO^- signatures through organic complexation. Despite these environmental contrasts, all four contexts ultimately yield carboxylate accumulation as a shared outcome. This convergence underscores that while the mechanisms differ, ranging from alkaline mineral exchange to acid-driven oxidation and organic complexation, the resulting spectral expressions reflect the universal instability of ester bonds and the adaptability of degradation pathways under diverse geochemical conditions.

The carbonate signals illustrate a similar interpretive tension. Bands at ~880-870 and 722–703 cm^{-1}, with accompanying higher-frequency shoulders in the ~1,470–1,420 cm^{-1} region, are strongest in cave and loess samples, consistent with mineral input and crust formation. Weak carbonate peaks are occasionally visible even in sandy or surface samples, as well. This raises the possibility that carbonate incorporation is not strictly environment-specific but may instead reflect microscale mineral contacts, local pH fluctuations, or even contamination. In this sense, carbonate bands are more reliable

as indicators of mineral involvement than as direct environmental markers, a point that bears caution when extending experimental findings to archaeological residues.

The frequent co-occurrence of carbonate fundamentals and carboxylate doublets in several specimens (e.g., 49-18 points 2–5; 49-44 points 1–6) suggests that mineral input is closely tied to adhesive transformation. This overlap implies that the progression from ester hydrolysis to stable carboxylate salts is not solely an intrinsic degradation pathway but is actively mediated by sediment chemistry (Karkanas et al., 2000; Weiner et al., 2002; Karkanas, 2010; Ortega-Villamagua et al., 2020; Suosaari et al., 2022). The presence of Ca- and Mg-rich crusts observed via SEM/EDS (Cnuts and Rots, 2024) supports this interpretation, indicating that mineral supply from the burial matrix plays a critical role in soap formation (Palacios and Monhemius, 2001; Ibrahim et al., 2005; Otero et al., 2014; Cotte et al., 2017; La Nasa et al., 2018; Filopoulou et al., 2021; Izzo et al., 2021; Thanaa, 2024; Poli et al., 2024).

Root processes may further amplify this effect (Weiner et al., 2002; Karkanas et al., 2000; Karkanas, 2010). Through the exudation of organic acids, roots can dissolve local carbonates and release divalent cations into porewaters, in turn accelerating residue alteration in rhizosphere-active soils (Ma et al., 2022; Ndzana et al., 2022; Ström et al., 2001; Tjelldén et al., 2015). In this sense, the carboxylate peaks observed in multiple samples may reflect both endogenous degradation of adhesive esters and exogenous contributions from sediment-root-residue interactions (Filopoulou et al., 2021; Otero et al., 2014; Weiner et al., 2002; Karkanas et al., 2000; Karkanas, 2010; Suosaari et al., 2022; Ortega-Villamagua et al., 2020; Ma et al., 2022; Ndzana et al., 2022). Recognizing this coupled mechanism complicates straightforward attribution but provides a more realistic multi-agent model of degradation that is highly relevant to archaeological contexts.

4.4 Biological processes

The influence of fungal and microbial activity, while less directly captured in FTIR spectra, emerges as an important secondary pathway (Child, 1995; Haslam, 2006; Schwarze, 2007; Turner-Walker, 2008; Pechal et al., 2013; Huisman et al., 2017; Hutschenreuther et al., 2017). SEM and EDS observations (Cnuts and Rots, 2024) document fungal penetration and mineral redistribution within several residues, particularly forest and cave contexts. These biological processes may explain some intra-sample heterogeneity in the OH and carboxylate regions, where patchy band intensities suggest localized biochemical alteration. While fungi and bacteria are likely accelerants of ester hydrolysis and oxidation, their signatures can be indirect and can easily overlap with mineral or chemical transformations (Ström et al., 2001; Lebon et al., 2010). As such, their role is inferred rather than proven in the present dataset, and their contribution as an important dimension of residue diagenesis remains supported by previous analysis.

Root activity constitutes a further potential pathway of residue alteration that intersects with both mineral and microbial processes. Roots exude a wide variety of compounds, including organic acids, sugars, and phenolics, which can acidify the surrounding matrix, mobilize cations, and stimulate microbial colonization (Ma et al., 2022; Ndzana et al., 2022; Ström et al., 2001; Tjelldén et al., 2015). In archaeological soils, root-derived oxalates are frequently implicated in carbonate dissolution and recrystallization (Ström et al., 2001; Tjelldén et al., 2015), while lignin and polysaccharide inputs may appear spectrally within the carbohydrate and C-O stretching regions (1,030–1,020 cm^{-1}). The localized shoulders in sample 49-52 near 1,320 cm^{-1} may plausibly correspond to oxalate salts, though overlap with other mineral phases complicates attribution. Similarly, polysaccharide-like signals in 49–30 and 49-42 could derive from root exudates as readily as from clay or silicate contaminants (Boeriu et al., 2004; Chambre and Dochia, 2021). The absence of consistent root-related features across all forest or loess samples suggests that root influence can be highly localized, likely depending on the proximity of existing plant life to residues at burial and on soil moisture habits that govern exudate transport.

From an archaeological perspective, recognizing potential root contributions is critical because their byproducts can mimic key degradation signatures. Oxalate precipitates, for instance, may overlap with carboxylate bands attributed to saponification, while polysaccharide contamination may complicate identification of resinous C-O stretches (Filopoulou et al., 2021; Otero et al., 2014; Boeriu et al., 2004; Chambre and Dochia, 2021). Without independent confirmation, such as through microscopic identification of root etching or oxalate crystal morphology, these features remain speculative. Nonetheless, their presence in some of the analyzed spectra highlights the importance of considering root processes alongside hydrolysis, oxidation, mineral accretion, and microbial activity when interpreting degraded organic residues in archaeological contexts.

The co-occurrence of carbonate absorptions and carboxylate bands within these specimens raises important interpretive challenges. While carbonate peaks have often been read as evidence of environmental encrustation (Weiner et al., 2002; Karkanas et al., 2000; Karkanas, 2010; Suosaari et al., 2022), the simultaneous intensity of COO^{-} stretches suggests coupled processes. Root systems, particularly in sandy and loessic soils, are known to exude organic acids that dissolve local carbonates (Ma et al., 2022; Ström et al., 2001; Tjelldén et al., 2015). This dissolution mobilizes Ca2+ and Mg2+, which can react with fatty and resin acids from the adhesives to form stable metal carboxylates (Filopoulou et al., 2021; Otero et al., 2014; Palacios and Monhemius, 2001; Ibrahim et al., 2005). Thus, residues in root-active soils may show both diminished ester carbonyls and enhanced carboxylate doublets, not solely from internal degradation but from root-sediment-residue interactions.

Such interactions may also explain some of the outlier cases: samples like 49-56, which lack strong carboxylates despite being in environments conducive to hydrolysis, may have been less directly exposed to root penetration or root-zone ion fluxes. By contrast, samples with pronounced carbonate-carboxylate coupling (such as 49-18, 49-44, and 49-48), may have been directly in contact with active rhizospheres where mineral solubilization and organic acid infiltration accelerated residue transformation.

This layered mechanism complicates interpretation in archaeological settings. Peaks at 1,560/1,415 cm^{-1} could derive from internal ester hydrolysis (saponification), from root-mediated ion mobilization, or from any combination of transformative processes. Similarly, carbonate absorptions should not be simplistically attributed to sedimentary overprinting alone,

since rhyzospheric carbonate cycling can leave indistinguishable signatures (Weiner et al., 2002; Karkanas et al., 2000; Karkanas, 2010; Ortega-Villamagua et al., 2020; Suosaari et al., 2022). Recognizing the intertwined roles of roots, sediments, and residues broadens the interpretive framework, shifting FTIR analysis from single-cause attribution toward a multi-agent model of degradation.

4.5 Pilot multivariate exploration

Multivariate analysis in this study highlights both its potential and its limitations. The PCA results indicate that raw reflectance spectra can produce patterns that loosely correspond to burial environments, whereas KKT-transformed spectra require additional preprocessing to achieve clearer separation. Yet, the small sample size (n = 9) and the high degree of intra-sample variability constrain the reliability of these outcomes. The sensitivity of clustering to specific preprocessing strategies also raises the possibility of overfitting, where apparent distinctions may reflect data treatment rather than genuine chemical differences. For these reasons, PCA in the present context should be regarded as an exploratory exercise; a methodological pilot that illustrates possible avenues for distinguishing degraded adhesives by depositional history. Here, it serves as a hypothesis-generating tool that underscores the need for expanded datasets and systematic experimental replication before robust classification models can be developed for archaeological applications.

4.6 Archaeological relevance and limitations

Taken together, the results show that spruce resin-beeswax adhesives degrade along multiple, overlapping pathways that cannot be reduced to a single model. Hydrolysis, oxidation, mineral incorporation, and microbial activity all play roles, but the relative contribution of each process varies unpredictably between samples and contexts. This complexity complicates efforts to assign residues to specific degradation stages or environments on the basis of FTIR alone. At the same time, the fact that many of these transformations align with patterns documented in archaeological materials, such as loss of esters, persistence of hydrocarbon stretches, soap formation, and carbonate encrustation, strengthens the relevance of the experimental data (Karkanas et al., 2000; Weiner et al., 2002; Mazza et al., 2006; Lombard, 2007; 2008; Vahur et al., 2011; Charrié-Duhaut et al., 2013; Helwig et al., 2014; Baales et al., 2017; Venditti et al., 2019; Luong et al., 2019; Kozowyk et al., 2020; Cnuts et al., 2022). Rather than providing a rigid interpretive template, this study offers a probabilistic outline: certain signatures are likely in particular settings, but outliers and exceptions must always be expected.

Many of these experimentally observed transformations parallel reports from archaeological contexts. For instance, the loss of ester carbonyls and persistence of lipidic hydrocarbon bands has been documented on hafting adhesives from Middle Stone Age and Upper Paleolithic assemblages as well as more recent materials (Lombard, 2007; 2008; Vahur et al., 2011; Charrié-Duhaut et al., 2013; Helwig et al., 2014; Venditti et al., 2019; Luong et al., 2019; Cnuts et al., 2022). Likewise, the occurrence of carboxylate doublets is consistent with soap formation described in organic acids, though their precise attribution has often remained uncertain (Palacios and Monhemius, 2001; Mirghani et al., 2002; Ibrahim et al., 2005; Cotte et al., 2017; Tiomno-Tiomnova et al., 2020; Filopoulou et al., 2021; Barannikov et al., 2024; Thanaa, 2024; Poli et al., 2024). By replicating these processes under controlled conditions, the present experiment provides a comparative framework for interpreting ambiguous archaeological spectra.

A further dimension that complicates residue interpretation is the possibility of contamination, both ancient and modern (Shanks et al., 2001; Monnier et al., 2013; Charrié-Duhaut et al., 2013; Pedergnana et al., 2016; Bordes et al., 2018; Croft et al., 2018; Pedergnana, 2020; Frahm et al., 2022). In burial contexts, residues may absorb humic acids, carbonates, or root-derived compounds that mimic or obscure endogenous chemical signals. For example, oxalates or polysaccharides introduced through plant root activity can overlap with adhesive-derived carboxylic or C–O stretches, making attribution uncertain (Ström et al., 2001; Boeriu et al., 2004; Tjelldén et al., 2015; Ma et al., 2022; Ndzana et al., 2022). Similarly, secondary mineral inputs, including calcite or gypsum from groundwater movement, can superimpose strong peaks that mask weaker organic bands (Karkanas et al., 2000; Weiner et al., 2002; Karkanas, 2010; Lebon et al., 2010; Ortega-Villamagua et al., 2020; Suosaari et al., 2022). Modern contamination is also a concern, particularly in settings where excavation, storage, or handling may introduce exogenous hydrocarbons, conservation materials, or residues from laboratory equipment (Craig and Collins, 2002; Monnier et al., 2013; Pedergnana et al., 2016; Bordes et al., 2018; Croft et al., 2018; Frahm et al., 2022). While precautions were taken in the present study to minimize such risks, the persistence of low-intensity or anomalous bands across some spectra raises the possibility that not all observed features derive from adhesive degradation alone (Shillito et al., 2009; Monnier et al., 2013; Pedergnana et al., 2016; Frahm et al., 2022). From an archaeological standpoint, recognizing and systematically accounting for potential contaminants is essential, since their spectral contributions may lead to overestimation of degradation processes or misidentification of functional residues (Rots et al., 2016; Wadley et al., 2004; Monnier et al., 2013; Pedergnana et al., 2016; Bordes et al., 2018; Croft et al., 2018; Hayes and Rots, 2019). Future experimental designs should therefore integrate contamination controls, such as clean blanks, environmental background spectra, and replication under sterile conditions, to better constrain the distinction between intrinsic degradation products and exogenous inputs.

Nevertheless, the limited sample size (n = 9) and the focus on a single adhesive mixture mean that these observations are limited in scope and should be regarded as exploratory rather than definitive. The trends identified here, while promising, remain broad hypotheses that require validation against larger experimental datasets and archaeological specimens.

5 Conclusion

The experimental degradation of spruce resin-beeswax adhesives explored here demonstrates both the persistence of diagnostic markers and the complexity of post-depositional

transformation. Hydrocarbon stretches from beeswax endure across all contexts, while ester carbonyl peaks diminish or are replaced by carboxylates, indicating active hydrolysis and soap formation. Carbonate and hydroxyl bands document mineral input and oxidative pathways, but their expression varies within environments, reflecting the strong influence of micro-scale conditions.

These results highlight the value of reflectance-mode FTIR microscopy for detecting both preserved and altered adhesive signatures in a non-destructive manner, while also cautioning against rigid interpretive templates. The variability across samples show that degradation pathways should be treated as probabilistic, shaped by sediment chemistry, microbial activity, and mineral contacts. PCA provides a promising means of differentiating preservation states, though its outcomes remain sensitive to preprocessing parameters and dataset size.

For archaeological applications, the findings reinforce the interpretive importance of recognizing transformative processes such as soap formation, carbonate incorporation, and oxidative shifts, while also acknowledging that their absence does not imply stability or lack of degradation. Rather than yielding fixed spectral models, this project contributes a non-deterministic framework for residue interpretation, suggesting that certain transformations are likely in particular contexts, but that of course outliers and exceptions should always be expected. This strengthens the methodological foundation for applying FTIR to archaeological adhesives, demonstrating how experimental degradation studies refine our ability to interpret complex residues in the deep past.

This study should be regarded as an exploratory proof-of-concept rather than a definitive statement on adhesive degradation pathways. The findings highlight key directions for future work, such as expanding the range of adhesive recipes, increasing sample sizes across varied burial environments, and integrating independent microscopic and chemical proxies to confirm FTIR-based inferences. By framing these results as a foundation rather than a final model, the study underscores the need for iterative, multi-method research to build a robust interpretive framework for archaeological residues.

Such expanded investigations will be critical for refining our ability to distinguish between residues derived from taphonomic processes versus those preserving authentic functional signatures. Ultimately, the archaeological relevance of this work lies in its capacity to translate insights from (laboratory) degradation experiments into improved interpretation of residues on ancient stone tools.

Data availability statement

The datasets presented in this study can be found in online repositories. The names of the repository/repositories and accession number(s) can be found in the article/Supplementary Material.

Author contributions

LL: Formal Analysis, Validation, Project administration, Methodology, Data curation, Supervision, Writing – original draft, Conceptualization, Funding acquisition, Writing – review and editing, Visualization, Software, Investigation, Resources. DC: Methodology, Conceptualization, Supervision, Writing – review and editing, Project administration. VR: Supervision, Writing – review and editing, Conceptualization, Methodology, Funding acquisition, Resources, Project administration.

Funding

The author(s) declared that financial support was received for this work and/or its publication. This research was made possible thanks to an equipment grant from the Fund for Scientific Research (F.R.S.-FNRS/EQP2023/U.N061.23) and the ARC research project GLUE ("Actions de Recherche Concertée", University of Liège), both attributed to VR. We are also indebted to the Fund for Scientific Research (F.R.S.-FNRS) and the University of Liège.

Acknowledgements

All experimental materials were produced at the University of Liège with the help of Christian Lepers, experienced primitive technologist.

Conflict of interest

The author(s) declared that this work was conducted in the absence of any commercial or financial relationships that could be construed as a potential conflict of interest.

Generative AI statement

The author(s) declared that generative AI was not used in the creation of this manuscript.

Any alternative text (alt text) provided alongside figures in this article has been generated by Frontiers with the support of artificial intelligence and reasonable efforts have been made to ensure accuracy, including review by the authors wherever possible. If you identify any issues, please contact us.

Publisher's note

Supplementary material

The Supplementary Material for this article can be found online at: https://www.frontiersin.org/articles/10.3389/fmats.2026.1764261/full#supplementary-material

References

Baales, M., Birker, S., and Mucha, F. (2017). Hafting with beeswax in the final Palaeolithic: a barbed point from bergkamen. *Antiquity* 91 (359), 1155–1170. doi:10.15184/aqy.2017.142

Barannikov, R., Vykydalová, A., Bezdička, P., Hermans, J., Plocek, J., and Švarcová, S. (2024). Thermal behavior of mercury carboxylates as paintings' degradation products. *J. Therm. Analysis Calorim.* 149 (23), 13773–13784. doi:10.1007/s10973-024-13463-3

Belbachir, K., Lecomte, S., Ta, H.-T., Petibois, C., and Desbat, B. (2011). Orientation of molecular groups of fibers in nonoriented samples determined by polarized ATR-FTIR spectroscopy. *Anal. Bioanal. Chem.* 401, 3263–3268. doi:10.1007/s00216-011-5418-0

Beltran, V. (2016). *Vibrational spectroscopies study of Pinus resin in materials from cultural heritage objects*.

Beltran, V., Salvado, N., Buti, S., and Pradell, T. (2016). Ageing of resin from Pinus species assessed by infrared spectroscopy. *Anal. Bioanal. Chem.* 408, 4073–4082. doi:10.1007/s00216-016-9496-x

Bertelli, I., Mattonai, M., La Nasa, J., and Ribechini, E. (2023). Study of thermal behavior and molecular composition of mixtures of resinous materials and beeswax found as adhesives in archaeological finds. *J. Anal. Appl. Pyrolysis.* 171, 105936. doi:10.1016/j.jaap.2023.105936

Boeriu, C. G., Bravo, D., Gosselink, R. J., and van Dam, J. E. (2004). Characterisation of structure-dependent functional properties of lignin with infrared spectroscopy. *Industrial Crops Prod.* 20 (2), 205–218. doi:10.1016/j.indcrop.2004.04.022

Bordes, L., Fullagar, R., Prinsloo, L. C., Hayes, E., Kozlikin, M. B., Shunkov, M. V., et al. (2018). Raman spectroscopy of lipid micro-residues on middle Palaeolithic stone tools from Denisova Cave, siberia. *J. Archaeol. Sci.* 95, 52–63. doi:10.1016/j.jas.2018.05.001

Briggs, D. E., and Summons, R. E. (2014). Ancient biomolecules: their origins, fossilization, and role in revealing the history of life. *BioEssays* 36 (5), 482–490. doi:10.1002/bies.201400010

Bruni, S., and Guglielmi, V. (2014). Identification of archaeological triterpenic resins by the non-separative techniques FTIR and 13C NMR: the case of pistacia resin (mastic) in comparison with frankincense. *Spectrochim. Acta A Mol. Biomol. Spectrosc.* 121, 613–622. doi:10.1016/j.saa.2013.10.098

Burroni, D., Donahue, R. E., Pollard, A. M., and Mussi, M. (2002). The surface alteration features of flint artefacts as a record of environmental processes. *J. Archaeol. Sci.* 29 (11), 1277–1287. doi:10.1006/jasc.2001.0771

Chambre, D. R., and Dochia, M. (2021). FT-IR characterization of cellulose crystallinity from raw bast fibers. Scientific and technical bulletin, series: chemistry. *Food Sci. Eng.* 18, 10–17.

Charrié-Duhaut, A., Porraz, G., Cartwright, C. R., Igreja, M., Connan, J., Poggenpoel, C., et al. (2013). First molecular identification of a hafting adhesive in the late howiesons poort at Diepkloof Rock Shelter (western cape, South Africa). *J. Archaeol. Sci.* 40, 3506–3518. doi:10.1016/j.jas.2012.12.026

Child, A. M. (1995). Towards an understanding of the microbial decomposition of archaeological bone in the burial environment. *J. Archaeol. Sci.* 22, 165–174. doi:10.1006/jasc.1995.0018

Čížová, K., Vizárová, K., Ház, A., Vykydalová, A., Cibulková, Z., and Šimon, P. (2019). Study of the degradation of beeswax taken from a real artefact. *J. Cult. Herit.* 37, 103–112. doi:10.1016/j.culher.2018.04.020

Colombini, M. P., and Modugno, F. (Eds.). (2009). *Organic mass spectrometry in art and archaeology*. John Wiley & Sons.

Cnuts, D., and Rots, V. (2018). Extracting residues from stone tools for optical analysis: towards an experiment-based protocol. *Archaeol. Anthropol. Sci.* 10 (7), 1717–1736. doi:10.1007/s12520-017-0484-7

Cnuts, D., and Rots, V. (2024). Examining the effect of post-depositional processes on the preservation and identification of stone tool residues from temperate environments: an experimental approach. *PLOS ONE* 19 (10), e0309060. doi:10.1371/journal.pone.0309060

Cnuts, D., Tomasso, S., and Rots, V. (2018). The role of fire in the life of an adhesive. *J. Archaeol. Method Theory* 25 (3), 839–862. doi:10.1007/s10816-017-9361-z

Cnuts, D., Peresani, M., and Rots, V. (2022). The contribution of stone tool residues in reconstructing Late Pleistocene hominin stone tool behaviour at Grotta di Fumane, Italy. *Quat. Sci. Rev.* 297, 107829. doi:10.1016/j.quascirev.2022.107829

Collins, M. J., Riley, M. S., Child, A. M., and Turner-Walker, G. (1995). A basic mathematical simulation of the chemical degradation of ancient collagen. *J. Archaeol. Sci.* 22 (2), 175–183. doi:10.1006/jasc.1995.0019

Cotte, M., Checroun, E., De Nolf, W., Taniguchi, Y., De Viguerie, L., Burghammer, M., et al. (2017). Lead soaps in paintings: friends or foes? *Stud. Conservation* 62 (1), 2–23. doi:10.1080/00393630.2016.1232529

Craig, O. E., and Collins, M. J. (2002). The removal of protein from mineral surfaces: implications for residue analysis of archaeological materials. *J. Archaeol. Sci.* 29 (10), 1077–1082. doi:10.1006/jasc.2001.0757

Croft, S. (2021). *Lithic residue analysis*. Oxford: BAR Publishing.

Croft, S., Monnier, G., Radini, A., Little, A., and Milner, N. (2016). Lithic residue survival and characterisation at star carr: a burial experiment. *Internet Archaeol.* 42. doi:10.11141/ia.42.5

Croft, S., Chatzipanagis, K., Kröger, R., and Milner, N. (2018). Misleading residues on lithics from star carr: identification with raman microspectroscopy. *J. Archaeol. Sci. Rep.* 19, 430–438. doi:10.1016/j.jasrep.2018.03.018

Daher, C., and Bellot-Gurlet, L. (2013). Non-destructive characterization of archaeological resins: seeking alteration criteria through vibrational signatures. *Anal. Methods* 5 (23), 6583–6591. doi:10.1039/c3ay41278d

Daher, C., Bellot-Gurlet, L., Le Hô, A. S., Paris, C., and Regert, M. (2013). Advanced discriminating criteria for natural organic substances of cultural heritage interest: spectral decomposition and multivariate analyses of FT-Raman and FT-IR signatures. *Talanta* 115, 540–547. doi:10.1016/j.talanta.2013.06.014

De Haseth, J. A., and Griffiths, P. (2007). *Fourier transform infrared spectrometry*. Wiley-Interscience.

Degano, I., Soriano, S., Villa, P., Pollarolo, L., Lucejko, J. J., Jacobs, Z., et al. (2019). Hafting of middle Paleolithic tools in latium (central Italy): new data from fossellone and Sant'Agostino caves. *PLoS ONE* 14 (6), e0213473. doi:10.1371/journal.pone.0213473

Denys, C. (2002). Taphonomy and experimentation. *Archaeometry* 44 (3), 469–484. doi:10.1111/1475-4754.00079

Derrick, M. R., Stulik, D., and Landry, J. M. (2000). *Infrared spectroscopy in conservation science*. Los Angeles, CA: Getty Conservation Institute.

Duce, C., Orsini, S., Spepi, A., Colombini, M. P., Rine, M. R., and Ribechini, E. (2015). Thermal degradation chemistry of archaeological pine pitch containing beeswax as an additive. *J. Anal. Appl. Pyrolysis* 111, 254–264. doi:10.1016/j.jaap.2014.10.020

Edwards, H. G., Farwell, D. W., and Daffner, L. (1996). Fourier-transform raman spectroscopic study of natural waxes and resins. I. *Spectrochimica Acta Part A Mol. Biomol. Spectrosc.* 52 (12), 1639–1648. doi:10.1016/0584-8539(96)01730-8

Eglinton, G., and Logan, G. A. (1991). Molecular preservation. *Philosophical Trans. R. Soc. B Biol. Sci.* 333 (1268), 315–328. doi:10.1098/rstb.1991.0081

Evershed, R. P. (1993). Biomolecular archaeology and lipids. *World Archaeol.* 25 (1), 74–93. doi:10.1080/00438243.1993.9980229

Evershed, R. P. (2008). Organic residue analysis in archaeology: the archaeological biomarker revolution. *Archaeometry* 50 (6), 895–924. doi:10.1111/j.1475-4754.2008.00446.x

Farmer, V. C. (1974). *The infrared spectra of minerals*, 4. London: Mineralogical Society, 51–67.

Favvas, E. P., Kouvelos, E. P., Papageorgiou, S. K., Tsanaktsidis, C. G., and Mitropoulos, A. C. (2015). Characterization of natural resin materials using water adsorption and various advanced techniques. *Appl. Phys. A* 119 (2), 735–743. doi:10.1007/s00339-015-9022-6

Filopoulou, A., Vlachou, S., and Boyatzis, S. C. (2021). Fatty acids and their metal salts: a review of their infrared spectra in light of their presence in cultural heritage. *Molecules* 26 (19), 6005. doi:10.3390/molecules26196005

Frahm, E., Adler, D. S., Gasparyan, B., Luo, B., Mallol, C., Pajović, G., et al. (2022). Every contact leaves a trace: documenting contamination in lithic residue studies at the middle Palaeolithic sites of lusakert cave 1 (armenia) and crvena stijena (montenegro). *PLOS ONE* 17 (4), e0266362. doi:10.1371/journal.pone.0266362

Gershenzon, J., and Dudareva, N. (2007). The function of terpene natural products in the natural world. *Nat. Chem. Biol.* 3 (7), 408–414. doi:10.1038/nchembio.2007.5

Goldberg, P. S., and Nathan, Y. (1975). The phosphate mineralogy of et-Tabun cave, mount Carmel, Israel. *Mineral. Mag.* 40 (311), 253–258. doi:10.1180/minmag.1975.040.311.06

Gregory, D., and Matthiesen, H. (2023). Defining the burial environment. *Handb. Archaeol. Sci.* 2, 1075–1088. doi:10.1002/9781119592112.ch53

Haslam, M. (2004). The decomposition of starch grains in soils: implications for archaeological residue analyses. *J. Archaeol. Sci.* 31 (12), 1715–1734. doi:10.1016/j.jas.2004.05.006

Hardy, B. L., Kay, M., Marks, A. E., and Monigal, K. (2001). "Stone tool function at the paleolithic sites of Starosele and Buran Kaya III, Crimea: Behavioral implications," in *Proceedings of the National Academy of Sciences* 98 (19), 10972-10977. doi:10.1073/pnas.191384498

Hardy, B. L., Moncel, M. H., Kerfant, C., Lebon, M., Bellot-Gurlet, L., and Mélard, N. (2020). Direct evidence of Neanderthal fibre technology and its cognitive and behavioral implications. *Sci. Rep.* 10 (1), 4889. doi:10.1038/s41598-020-61839-w

Haslam, M. (2006). Potential misidentification of *in situ* archaeological tool-residues: starch and conidia. *J. Archaeol. Sci.* 33 (1), 114–121. doi:10.1016/j.jas.2005.07.004

Hayes, E., and Rots, V. (2019). Documenting scarce and fragmented residues on stone tools: an experimental approach using optical microscopy and SEM-EDS. *Archaeol. Anthropol. Sci.* 11 (7), 3065–3099. doi:10.1007/s12520-018-0736-1

Hayes, E., Cnuts, D., and Rots, V. (2019). Integrating SEM-EDS in a sequential residue analysis protocol: benefits and challenges. *J. Archaeol. Sci. Rep.* 23, 116–126. doi:10.1016/j.jasrep.2018.10.029

Helwig, K., Monahan, V., Poulin, J., and Andrews, T. D. (2014). Ancient projectile weapons from ice patches in northwestern Canada: identification of resin and compound resin-ochre hafting adhesives. *J. Archaeol. Sci.* 41, 655–665. doi:10.1016/j.jas.2013.09.010

High, K., Milner, N., Panter, I., and Penkman, K. E. H. (2015). Apatite for destruction: investigating bone degradation due to high acidity at Star Carr. *J. Archaeol. Sci.* 59, 159–168. doi:10.1016/j.jas.2015.04.001

Huber, B., Vassão, D. G., Roberts, P., Wang, Y. V., and Larsen, T. (2022). Chemical modification of biomarkers through accelerated degradation: implications for ancient plant identification in archaeo-organic residues. *Molecules* 27 (10), 3331. doi:10.3390/molecules27103331

Huisman, H., Ismail-Meyer, K., Sageidet, B. M., and Joosten, I. (2017). Micromorphological indicators for degradation processes in archaeological bone from temperate European wetland sites. *J. Archaeol. Sci.* 85, 13–29. doi:10.1016/j.jas.2017.06.016

Hutschenreuther, A., Watzke, J., Schmidt, S., Büdel, T., and Henry, A. G. (2017). Archaeological implications of the digestion of starches by soil bacteria: interaction among starches leads to differential preservation. *J. Archaeol. Sci. Rep.* 15, 95–108. doi:10.1016/j.jasrep.2017.07.006

Ibrahim, M., Nada, A., and Kamal, D. E. (2005). Density functional theory and FTIR spectroscopic study of carboxyl group. *Indian J. Pure Appl. Phys.* 44 (12), 911–917.

Izzo, F., Germinario, C., Grifa, C., Langella, A., and Mercurio, M. (2020). External reflectance FTIR dataset (4000-400 cm-1) for the identification of relevant mineralogical phases forming cultural heritage materials. *Infrared Phys. Technol.* 106, 103266. doi:10.1016/j.infrared.2020.103266

Izzo, F. C., Kratter, M., Nevin, A., and Zendri, E. (2021). A critical review on the analysis of metal soaps in oil paintings. *ChemistryOpen* 10 (9), 904–921. doi:10.1002/open.202100166

Karkanas, P. (2010). Preservation of anthropogenic materials under different geochemical processes: a mineralogical approach. *Quat. Int.* 214, 63–69. doi:10.1016/j.quaint.2009.10.017

Karkanas, P., Bar-Yosef, O., Goldberg, P., and Weiner, S. (2000). Diagenesis in prehistoric caves: the use of minerals that form *in situ* to assess the completeness of the archaeological record. *J. Archaeol. Sci.* 27 (10), 915–929. doi:10.1006/jasc.1999.0506

Karkanas, P., Rigaud, J. P., Simek, J. F., Albert, R. M., and Weiner, S. (2002). Ash, bones and guano: a study of the minerals and phytoliths in the sediments of grotte XVI, Dordogne, France. *J. Archaeol. Sci.* 29 (7), 721–732. doi:10.1006/jasc.2001.0742

Kozowyk, P. R. B., Poulis, J. A., and Langejans, G. H. J. (2017). Laboratory strength testing of pine wood and birch bark adhesive: a first study of the material properties of pitch. *J. Archaeol. Sci. Rep.* 13, 49–59. doi:10.1016/j.jasrep.2017.03.006

Kozowyk, P. R. B., van Gijn, A. L., and Langejans, G. H. J. (2020). Understanding preservation and identification biases of ancient adhesives through experimentation. *Archaeol. Anthropol. Sci.* 12, 209. doi:10.1007/s12520-020-01179-y

Kozowyk, P. R., Poulis, J. A., and Langejans, G. H. (2025). Suberin-related bands identified with FTIR are unreliable to differentiate neanderthal tar production strategies. *J. Paleolithic Archaeol.* 8 (1), 41. doi:10.1007/s41982-025-00249-8

La Nasa, J., Lluveras-Tenorio, A., Modugno, F., and Bonaduce, I. (2018). Two-step analytical procedure for the characterization and quantification of metal soaps and resinates in paint samples. *Herit. Sci.* 6, 57. doi:10.1186/s40494-018-0222-1

Langejans, G. H. (2010). Remains of the day—preservation of organic micro-residues on stone tools. *J. Archaeol. Sci.* 37 (5), 971–985. doi:10.1016/j.jas.2009.11.030

Langejans, G., Aleo, A., Fajardo, S., and Kozowyk, P. (2022). "Archaeological adhesives," in *Oxford research encyclopedia of anthropology*.

Lebon, M., Reiche, I., Bahain, J. J., Chadefaux, C., Moigne, A. M., Fröhlich, F., et al. (2010). New parameters for the characterization of diagenetic alterations and heat-induced changes of fossil bone mineral using fourier transform infrared spectrometry. *J. Archaeol. Sci.* 37 (9), 2265–2276. doi:10.1016/j.jas.2010.03.024

Lerchi, A., Krap, T., Eppenberger, P., and Pedergnana, A. (2022). Implementation of adipocere fingerprinting in archaeology by applying a forensic approach. *TrAC Trends Anal. Chem.* 157, 116801. doi:10.1016/j.trac.2022.116801

Liu, X. Y., Timar, M. C., and Varodi, A. M. (2019). A comparative study on the artificial UV and natural ageing of beeswax and Chinese wax and influence of wax finishing on the ageing of Chinese ash (Fraxinus mandshurica) wood surfaces. *J. Photochem. Photobiol. B Biol.* 201, 111607. doi:10.1016/j.jphotobiol.2019.111607

Lombard, M. (2007). The gripping nature of ochre: the association of ochre with howiesons poort adhesives and later stone age mastics from South Africa. *J. Hum. Evol.* 53, 406–419. doi:10.1016/j.jhevol.2007.05.004

Lombard, M. (2008). Finding resolution for the howiesons poort through the microscope: micro-residue analysis of segments from Sibudu Cave, South Africa. *J. Archaeol. Sci.* 35, 26–41. doi:10.1016/j.jas.2007.02.021

Łucejko, J. J., Mattonai, M., Zborowska, M., Tamburini, D., Cofta, G., Cantisani, E., et al. (2018). Deterioration effects of wet environments and brown rot fungus *Coniophora puteana* on pine wood in the archaeological site of biskupin (poland). *Microchem. J.* 138, 132–146. doi:10.1016/j.microc.2017.12.028

Luong, S., Tocheri, M. W., Hayes, E., Sutikna, T., Fullagar, R., Saptomo, E. W., et al. (2019). Combined organic biomarker and use-wear analyses of stone artefacts from liang Bua, Flores, Indonesia. *Sci. Rep.* 9 (1), 17553. doi:10.1038/s41598-019-53782-2

Ma, W., Tang, S., Dengzeng, Z., Zhang, D., Zhang, T., and Ma, X. (2022). Root exudates contribute to belowground ecosystem hotspots: a review. *Front. Microbiol.* 13, 937940. doi:10.3389/fmicb.2022.937940

Martín Ramos, P., Ruíz Potosme, N. M., Fernández Coppel, I. A., and Martín Gil, J. (2018). *Potential of ATR-FTIR spectroscopy for the classification of natural resins (No. ART-2018-106905)*. doi:10.5530/bems.4.1.2

Martín-Viveros, J. I., and Ollé, A. (2020). Using 3D digital microscopy and SEM-EDX for in-situ residue analysis: a multi-analytical contextual approach on experimental stone tools. *Quat. Int.* 569, 228–262. doi:10.1016/j.quaint.2020.06.046

Mazurek, J., Svoboda, M., and Schilling, M. (2019). GC/MS characterization of beeswax, protein, gum, resin, and oil in romano-egyptian paintings. *Heritage* 2 (3), 1960–1985. doi:10.3390/heritage2030119

Mazza, P. P. A., Martini, F., Sala, B., Magi, M., Colombini, M. P., Giachi, G., et al. (2006). A new Palaeolithic discovery: tar-hafted stone tools in a european mid-pleistocene bone-bearing bed. *J. Archaeol. Sci.* 33 (9), 1310–1318. doi:10.1016/j.jas.2006.01.006

Mercurio, M., Rossi, M., Izzo, F., Cappelletti, P., Germinario, C., Grifa, C., et al. (2018). The characterization of natural gemstones using non-invasive FT-IR spectroscopy: new data on tourmalines. *Talanta* 178, 147–159. doi:10.1016/j.talanta.2017.09.030

Michel, M., and Rots, V. (2022). Into the light: the effect of UV light on flint tool surfaces, residues and adhesives. *J. Archaeol. Sci. Rep.* 43, 103479. doi:10.1016/j.jasrep.2022.103479

Michel, M., Cnuts, D., and Rots, V. (2019). Freezing in-sight: the effect of frost cycles on use-wear and residues on flint tools. *Archaeol. Anthropol. Sci.* 11 (10), 5423–5443. doi:10.1007/s12520-019-00881-w

Miłek, M., Drogoń, A., Pyda, M., Czerniecka-Kubicka, A., Tomczyk, M., and Dżugan, M. (2020). The use of infrared spectroscopy and thermal analysis for the quick detection of adulterated beeswax. *J. Apic. Res.* 59 (4), 677–684. doi:10.1080/00218839.2020.1773037

Mirghani, M. E., Che Man, Y. B., Jinap, S., Baharin, B. S., and Bakar, J. (2002). FTIR spectroscopic determination of soap in refined vegetable oils. *J. Am. Oil Chemists' Soc.* 79 (2), 111–116. doi:10.1007/s11746-002-0443-4

Monico, L., Rosi, F., Miliani, C., Daveri, A., and Brunetti, B. G. (2013). Non-invasive identification of metal-oxalate complexes on polychrome artwork surfaces by reflection mid-infrared spectroscopy. *Spectrochim. Acta A* 116, 270–280. doi:10.1016/j.saa.2013.06.084

Monnier, G., and May, K. (2019). Documenting the degradation of animal-tissue residues on experimental stone tools: a multianalytical approach. *Archaeol. Anthropol. Sci.* 11, 6803–6827. doi:10.1007/s12520-019-00941-1

Monnier, G. F., Hauck, T. C., Feinberg, J. M., Luo, B., Le Tensorer, J. M., and Al Sakhel, H. (2013). A multi-analytical methodology of lithic residue analysis applied to Paleolithic tools from hummal, Syria. *J. Archaeol. Sci.* 40 (10), 3722–3739. doi:10.1016/j.jas.2013.03.018

Monnier, G., Frahm, E., Luo, B., and Missal, K. (2017). Developing FTIR microspectroscopy for analysis of plant residues on stone tools. *J. Archaeol. Sci.* 78, 158–178. doi:10.1016/j.jas.2016.12.004

Monnier, G., Frahm, E., Luo, B., and Missal, K. (2018). Developing FTIR microspectroscopy for the analysis of animal-tissue residues on stone tools. *J. Archaeol. Method Theory* 25 (1), 1–44. doi:10.1007/s10816-017-9325-3

Ndzana, G. M., Zhang, Y., Yao, S., Hamer, U., and Zhang, B. (2022). The adsorption capacity of root exudate organic carbon onto clay mineral surface changes depending on clay mineral types and organic carbon composition. *Rhizosphere* 23, 100545. doi:10.1016/j.rhisph.2022.100545

Nicholson, R. A. (1998). Bone degradation in a compost heap. *J. Archaeol. Sci.* 25 (5), 393–403. doi:10.1006/jasc.1997.0208

Nielsen-Marsh, C. M., and Hedges, R. E. (2000). Patterns of diagenesis in bone I: the effects of site environments. *J. Archaeol. Sci.* 27 (12), 1139–1150. doi:10.1006/jasc.1999.0537

Nunziante-Cesaro, S., and Lemorini, C. (2012). The function of prehistoric lithic tools: a combined study of use-wear analysis and FTIR microspectroscopy. *Spectrochim. Acta A* 86, 299–304. doi:10.1016/j.saa.2011.10.040

Ortega-Villamagua, E., Gudiño-Gomezjurado, M., and Palma-Cando, A. (2020). Microbiologically induced carbonate precipitation in the restoration and conservation of cultural heritage materials. *Molecules* 25 (23), 5499. doi:10.3390/molecules25235499

Otero, V., Sanches, D., Montagner, C., Vilarigues, M., Carlyle, L., Lopes, J. A., et al. (2014). Characterisation of metal carboxylates by raman and infrared spectroscopy in works of art. *J. Raman Spectrosc.* 45 (11–12), 1197–1206. doi:10.1002/jrs.4520

Palacios, E. G., and Monhemius, A. J. (2001). Infrared spectroscopy of metal carboxylates: I. Determination of free acid in solution. *Hydrometallurgy* 62 (3), 135–143. doi:10.1016/s0304-386x(01)00187-6

Pechal, J. L., Crippen, T. L., Tarone, A. M., Lewis, A. J., Tomberlin, J. K., and Benbow, M. E. (2013). Microbial community functional change during vertebrate carrion decomposition. *PLOS ONE* 8 (11), e79035. doi:10.1371/journal.pone.0079035

Pedergnana, A. (2020). All that glitters is not gold: evaluating the nature of the relationship between archaeological residues and stone tool function. *J. Paleolit. Archaeol.* 3, 225–254. doi:10.1007/s41982-019-00039-z

Pedergnana, A., and Ollé, A. (2018). Building an experimental comparative reference collection for lithic micro-residue analysis based on a multi-analytical approach. *J. Archaeol. Method Theory* 25 (1), 117–154. doi:10.1007/s10816-017-9337-z

Pedergnana, A., Asryan, L., Fernández-Marchena, J. L., and Ollé, A. (2016). Modern contaminants affecting microscopic residue analysis on stone tools: a word of caution. *Micron* 86, 1–21. doi:10.1016/j.micron.2016.04.003

Piña-Torres, C., Lucero-Gomez, P., Nieto, S., Vazquez, A., Bucio, L., Belio, I., et al. (2018). An analytical strategy based on fourier transform infrared spectroscopy, principal component analysis and linear discriminant analysis to suggest the botanical origin of resins from bursera. Application to archaeological Aztec samples. *J. Cult. Herit.* 33, 48–59. doi:10.1016/j.culher.2018.02.006

Pokines, J. T., Faillace, K., Berger, J., Pirtle, D., Sharpe, M., Curtis, A., et al. (2018). The effects of repeated wet-dry cycles as a component of bone weathering. *J. Archaeol. Sci. Rep.* 17, 433–441. doi:10.1016/j.jasrep.2017.11.025

Poli, T., Haaf, M. P., Piccirillo, A., Costa, A. P., Craig, R. L., and Pozzi, F. (2024). First insights into the formation of metal soaps in alkyd-based paints: a proof-of-concept investigation using FTIR spectroscopy. *Molecules* 29 (24), 5840. doi:10.3390/molecules29245840

Prinsloo, L. C., Wadley, L., and Lombard, M. (2014). Infrared reflectance spectroscopy as an analytical technique for the study of residues on stone tools: potential and challenges. *J. Archaeol. Sci.* 41, 732–739. doi:10.1016/j.jas.2013.10.011

Regert, M. (2004). Investigating the history of prehistoric glues by gas chromatography–mass spectrometry. *J. Sep. Sci.* 27 (3), 244–254. doi:10.1002/jssc.200301608

Regert, M., Colinart, S., Degrand, L., and Decavallas, O. (2001). Chemical alteration and use of beeswax through time: accelerated ageing tests and analysis of archaeological samples from various environmental contexts. *Archaeometry* 43 (4), 549–569. doi:10.1111/1475-4754.00036

Rots, V. (2003). Towards an understanding of hafting: the macro- and microscopic evidence. *Antiquity* 77 (298), 805–815. doi:10.1017/s0003598x00061743

Rots, V. (2010). *Prehension and hafting traces on flint tools: a methodology. Universitaire pers leuven*.

Rots, V., Hayes, E., Cnuts, D., Lepers, C., and Fullagar, R. (2016). Making sense of residues on flaked stone artefacts: learning from blind tests. *PLOS ONE* 11 (3), e0150437. doi:10.1371/journal.pone.0150437

Russo, S., Brambilla, L., Thomas, J. B., and Joseph, E. (2023). But aren't all soaps metal soaps? A review of applications, physico-chemical properties of metal soaps and their occurrence in cultural heritage studies. *Herit. Sci.* 11, 172. doi:10.1186/s40494-023-00988-3

Saitta, E. T., and Kaye, T. G. (2025). Experimental maturation of pine resin in sediment to investigate the formation of synthetic copal and amber. *Sci. Rep.* 15 (1), 7627. doi:10.1038/s41598-025-89448-5

Sano, K., Arrigi, S., Stani, C., Aureli, D., Boschin, F., Fiore, I., et al. (2019). The earliest evidence for mechanically delivered projectile weapons in Europe. *Nat. Ecol. Evol.* 3 (10), 1409–1414. doi:10.1038/s41559-019-0990-3

Scaggion, C., Dal Sasso, G., Nodari, L., Pagani, L., Carrara, N., Zotti, A., et al. (2024). An FTIR-Based model for the diagenetic alteration of archaeological bones. *J. Archaeol. Sci.* 161, 105900. doi:10.1016/j.jas.2023.105900

Schmidt, P., and Koch, T. J. (2024). The molecular composition of birch tar and its infrared spectrum. *Archaeol. Anthropol. Sci.* 16 (12), 193. doi:10.1007/s12520-024-02102-5

Schmidt, P., Blessing, M., Rageot, M., Iovita, R., Pfleging, J., Nickel, K. G., et al. (2019). "Birch tar production does not prove Neanderthal behavioral complexity." in *Proceedings of the National Academy of Sciences* 116 (36), 17707-17711. doi:10.1073/pnas.1911137116

Schwarze, F. W. (2007). Wood decay under the microscope. *Fungal Biol. Rev.* 21, 133–170. doi:10.1016/j.fbr.2007.09.001

Shanks, O. C., Bonnichsen, R., Vella, A. T., and Ream, W. (2001). Recovery of protein and DNA trapped in stone tool microcracks. *J. Archaeol. Sci.* 28 (9), 965–972. doi:10.1006/jasc.2000.0628

Shillito, L. M., Almond, M. J., Wicks, K., Marshall, L. J. R., and Matthews, W. (2009). The use of FT-IR as a screening technique for organic residue analysis of archaeological samples. *Spectrochimica Acta Part A Mol. Biomol. Spectrosc.* 72 (1), 120–125. doi:10.1016/j.saa.2008.08.016

Socrates, G. (2004). *Infrared and raman characteristic group frequencies: tables and charts*. John Wiley & Sons.

Solodenko, N., Zupancich, A., Cesaro, S. N., Marder, O., Lemorini, C., and Barkai, R. (2015). Fat residue and use-wear found on Acheulian biface and scraper associated with butchered elephant remains at the site of Revadim, Israel. *PloS One* 10 (3), e0118572. doi:10.1371/journal.pone.0118572

Ström, L., Owen, A. G., Godbold, D. L., and Jones, D. L. (2001). Organic acid behaviour in a calcareous soil: sorption reactions and biodegradation rates. *Soil Biol. Biochem.* 33, 2125–2133. doi:10.1016/s0038-0717(01)00146-8

Stuart, B. (2021). *Infrared spectroscopy. Analytical techniques in forensic science*, 145-160. doi:10.1002/9781119373421.ch7

Suosaari, E. P., Lascu, I., Oehlert, A. M., Parlanti, P., Mugnaioli, E., Gemmi, M., et al. (2022). Authigenic clays as precursors to carbonate precipitation in saline lakes of Salar de Llamara, Northern Chile. *Commun. Earth & Environ.* 3 (1), 325. doi:10.1038/s43247-022-00658-5

Tanner, N., and Lichtenberg-Kraag, B. (2019). Identification and quantification of single and multi-adulteration of beeswax by FTIR-ATR spectroscopy. *Eur. J. Lipid Sci. Technol.* 121 (12), 1900245. doi:10.1002/ejlt.201900245

Tappert, R., Wolfe, A. P., McKellar, R. C., Tappert, M. C., and Muehlenbachs, K. (2011). Characterizing modern and fossil gymnosperm exudates using micro-Fourier transform infrared spectroscopy. *Int. J. Plant Sci.* 172 (1), 120-138. doi:10.1086/657277

Teacă, C. A., Roşu, D., Bodîrlău, R., and Roşu, L. (2013). Structural changes in wood under artificial UV light irradiation determined by FTIR spectroscopy and color Measurements—a brief review. *BioResources* 8 (1). doi:10.15376/biores.8.1.1478-1507

Thanaa, A., Sumayli, M., and El-Shabasy, A. (2024). Biodegradation effects of three Aspergillus species on iron-based oxides (Hematite – Goethite) in paint layer in oil paintings. *Saudi J. Biol. Sci.* 31 (7), 104004. doi:10.1016/j.sjbs.2024.104004

Tiomno-Tiomnova, O., Rodriguez-Chanfrau, J. E., Gamiotea-Turro, D., Silva, T. S., Martins, C. H. G., Valerino-Diaz, A., et al. (2020). *Obtaining salts of resin acids from Cuban pine by metathesis reactions*.

Tjelldén, A. K. E., Kristiansen, S. M., Matthiesen, H., and Pedersen, O. (2015). Impact of roots and rhizomes on wetland archaeology: a review. *Conservation Manag. Archaeol. Sites* 17 (4), 370–391. doi:10.1080/13505033.2016.1175909

Toffolo, M. (2025). *Infrared spectroscopy of archaeological sediments*. Cambridge University Press.

Tollan, P., Ellis, B., Troch, J., and Neukampf, J. (2019). Assessing magmatic volatile equilibria through FTIR spectroscopy of unexposed melt inclusions and their host quartz: a new technique and application to the Mesa falls tuff, yellowstone. *Contributions Mineralogy Petrology* 174 (3), 24. doi:10.1007/s00410-019-1561-y

Turner-Walker, G. (2008). "The chemical and microbial degradation of bones and teeth," in *Advances in human palaeopathology*, 3–29.

Vahur, S., Kriiska, A., and Leito, I. (2011). Investigation of the adhesive residue on the flint insert and the adhesive lump found from the pulli early Mesolithic settlement site (estonia) by micro-ATR-FT-IR spectroscopy. *Est. J. Archaeol.* 15 (1), 3–17. doi:10.3176/arch.2011.1.01

Van Nimmen, E., De Clerck, K., Verschuren, J., Gellynck, K., Gheysens, T., Mertens, J., et al. (2008). FT-IR spectroscopy of spider and silkworm silks part I. Different sampling techniques. *Vib. Spectrosc.* 46, 63–68. doi:10.1016/j.vibspec.2007.10.003

Venditti, F., Cristiani, E., Nunziante-Cesaro, S., Agam, A., Lemorini, C., and Barkai, R. (2019). Animal residues found on tiny lower Paleolithic tools reveal their use in butchery. *Sci. Rep.* 9 (1), 13031. doi:10.1038/s41598-019-49650-8

Wadley, L. (2010). Compound-adhesive manufacture as a common behavioural proxy for complex cognition in the Middle Stone Age. *Curr. Anthropol.* 51 (1), S111–S119. doi:10.1086/649836

Wadley, L., Lombard, M., and Williamson, B. (2004). The first residue analysis blind tests: results and lessons learnt. *J. Archaeol. Sci.* 31 (11), 1491–1501. doi:10.1016/j.jas.2004.03.010

Weiner, S. (2010). *Microarchaeology: beyond the visible archaeological record*. Cambridge: Cambridge University Press. doi:10.1017/CBO9780511811210

Weiner, S., Goldberg, P., and Bar-Yosef, O. (2002). Three-dimensional distribution of minerals in the sediments of hayonim Cave, Israel: diagenetic processes and archaeological implications. *J. Archaeol. Sci.* 29 (11), 1289–1308. doi:10.1006/jasc.2001.0790

Williamson, B. S. (2004). Middle Stone Age tool function from residue analysis at Sibudu Cave. *South Afr. J. Sci.* 100, 174–179.

Wilson, L. Y. N., and Pollard, A. M. (2002). Here today, gone tomorrow? Integrated experimentation and geochemical modeling in studies of archaeological diagenetic change. *Accounts Chem. Res.* 35 (8), 644–651. doi:10.1021/ar000203s

Wilson, A. S., Dodson, H. I., Janaway, R. C., Pollard, A. M., and Tobin, D. J. (2007). Selective biodegradation in hair shafts derived from archaeological, forensic, and experimental contexts. *Br. J. Dermatology* 157, 450–457. doi:10.1111/j.1365-2133.2007.07973.x

Wragg Sykes, R. M. (2015). "To see a world in a hafted tool: birch pitch composite technology, cognition, and memory in neanderthals," in *Settlement, society and cognition in human evolution*. Editors F. S. Coward, R. Hosfield, M. Pope, and F. Wenban-Smith

Zurro, D., and Gadekar, C. (2024). Is it worth it? A review of plant residue analysis on knapped lithic artifacts. *Lithic Technol.* 49 (1), 63–80. doi:10.1080/01977261.2023.2188343